
The Limitations of Large Width in Neural Networks: A Deep Gaussian Process Perspective

Geoff Pleiss
Columbia University
gmp2162@columbia.edu

John P. Cunningham
Columbia University
jpc2181@columbia.edu

Abstract

Large width limits have been a recent focus of deep learning research: modulo computational practicalities, do wider networks outperform narrower ones? Answering this question has been challenging, as conventional networks gain representational power with width, potentially masking any negative effects. Our analysis in this paper decouples capacity and width via the generalization of neural networks to Deep Gaussian Processes (Deep GP), a class of hierarchical models that subsume neural nets. In doing so, we aim to understand how width affects standard neural networks once they have sufficient capacity for a given modeling task. Our theoretical and empirical results on Deep GP suggest that *large width is generally detrimental to hierarchical models*. Surprisingly, we prove that even nonparametric Deep GP converge to Gaussian processes, effectively becoming shallower without any increase in representational power. The posterior, which corresponds to a mixture of data-adaptable basis functions, becomes less data-dependent with width. Our tail analysis demonstrates that width and depth have opposite effects: depth accentuates a model’s non-Gaussianity, while width makes models increasingly Gaussian. We find there is a “sweet spot” that maximizes test set performance before the limiting GP behavior prevents adaptability, occurring at width = 1 or width = 2 for nonparametric Deep GP. These results make strong predictions about the same phenomenon in conventional neural networks: we show empirically that many neural network architectures need 10 – 500 hidden units for sufficient capacity—depending on the dataset—but further width degrades test performance.

1 Introduction

Research has shown that deeper neural networks tend to be more expressive and efficient than wider networks under a variety of metrics [e.g. 19, 56, 60, 63, 67, 68, 71, 76]. Nevertheless, there is resurgent interest in wide models due in part to empirical successes [e.g. 84] and theoretical analyses of limiting behavior. When randomly initialized to create a distribution over functions, neural networks converge to Gaussian processes (GP) as width increases. This result, first proved for 2-layer networks [62], has been extended to deeper networks [49, 57], convolutional networks [35, 64], and other architectures [44, 80]. A similar limit exists for gradient-trained networks, which behave increasingly like kernel machines under the neural tangent kernel [e.g. 5, 7, 26, 45, 50, 81].

While these limits simplify analyses, there is something unsettling about reducing neural networks to kernel methods. Neal [62, p. 161] describes the GP limit as “disappointing,” noting that “infinite networks do not have hidden units that represent ‘hidden features’ . . . often seen [as the] interesting aspect of neural network learning.” Recent work indeed shows that learned hierarchical features can be exponentially more efficient than the fixed shallow representations of kernels [e.g. 3, 4, 7, 10, 12, 19, 37, 38, 53, 83]. At the same time, wider networks can more accurately model complex functions [40]. Thus, wide limits appear to confound opposing phenomenon: increased capacity makes them

more expressive, yet the loss of hierarchical features seems to make them less expressive. This may explain the mixed empirical performance of limiting models: outperforming finite width models in some scenarios [e.g. 8, 35, 51], yet falling short on more complex tasks [e.g. 7, 10, 32, 50, 74].

This paper aims to decouple these effects of large width. Our goal is to understand the inductive biases of wide networks, after a network has “sufficient” capacity for a given modeling task. We ask: *If we control for the effects of increased capacity, what—if any—value remains in wide networks?*

To achieve this control, we note that a typical neural network layer corresponds to a finite basis, where elementwise nonlinearities transform each hidden feature into a *single basis function*. In order to decouple width from capacity, one could generalize these layers so that each nonlinearity produces any number of basis functions; if each hidden feature gives rise to an infinite and universal basis, then hidden layers would have infinite representational capacity *regardless of width*. This generalization is in fact a well-studied class of hierarchical models—Deep Gaussian Processes (**Deep GP**) [17, 22, 24, 25, 28, 30, 41, 72]—where standard neural net layers are replaced with vector-valued Gaussian processes. Indeed, typical neural networks are a degenerate Deep GP subclass [1, 2, 31, 65].

We therefore have a generalization of neural networks where capacity is controlled, from which we can glean insights about conventional networks that have sufficient representational power for a given modeling task. Surprisingly, despite using Gaussian processes as the primary hierarchical component, we prove that *Deep GP converge to (single-layer) GP in their infinite width limit* (Thm. 1). Troubling implications immediately ensue: large width is strictly detrimental to Deep GP, as the limiting model collapses to a shallower version of itself. We support this theorem with an analysis of neural network and Deep GP posteriors, which *become less adaptable as width increases*. Specifically, we show that the posterior mean corresponds to a mixture of functions drawn from data-dependent (and thus adaptive) reproducing kernel Hilbert spaces, formalizing the above claim from Neal [62]. As width increases, this mixture collapses to the data-independent kernel of the limiting GP, implying that wider models have less feature learning. Finally, we present a novel tail analysis which indicates that *width and depth have opposite effects*: depth accentuates non-Gaussianity, sharpening peaks and fattening tails, whereas width increases Gaussianity (Thms. 2 and 3).

Our theoretical results hold for Deep GP and conventional (parametric) neural networks alike. Experiments confirm that—after a model achieves sufficient capacity—*width becomes harmful to model fit and performance*. For nonparametric Deep GP, a width of 1 or 2 often achieves the best performance and fit. Neural networks naturally require more hidden units; nevertheless, performance degrades after a certain width. On small datasets ($N \leq 1000$) with low dimensionality, we find that models with ≤ 16 hidden units achieve best test set performance. On larger datasets like CIFAR10, this “sweet spot” occurs later (at ≈ 500 hidden units for sufficiently deep models), yet performance degrades beyond this width. Our findings strongly suggest that narrower models have better inductive biases, and wide models perform well *in spite of*—not because of—large width.

2 Setup

2.1 Related Work

Effects of width. Works have shown that, given finite parameters, deeper models are more expressive than wider models [56, 60, 67, 68, 76]. Similarly to our work, Aitchison [2] shows that width potentially harms prior and posterior expressivity of deep linear models. Nevertheless, wide models have been shown to have favorable optimization landscapes [6, 26, 52, 63, 75] and are resistant to overfitting via double descent [11, 18, 61]. Our work controls for these factors by examining nonparametric hierarchical models with exact Bayesian inference, and thus does not disagree with these other works. Infinite width limits have received renewed interest in Bayesian [35, 44, 50, 57, 62, 64, 80] and non-Bayesian [5, 7, 20, 26, 39, 45, 50, 58, 81, 82] settings. Most of these works show that neural networks converge to kernel methods, though recent work suggests that this limiting behavior can be avoided with different parameterizations [e.g. 20, 39, 58, 82]. Similarly to Lee et al. [50], our Deep GP limit analysis sequentially increases the width of each layer, though we hypothesize a similar proof exists where the width of all layers increases simultaneously (akin to [57]).

Deep GP are introduced by Damianou and Lawrence [25]. A large portion of Deep GP research has thus far focused on scalable approximate inference methods [17, 22, 23, 30, 41, 65, 72, 78]. Though prior work has studied tail properties of neural networks [77, 85] and Deep GP with RBF

kernels [55], our work is—to the best of our knowledge—the first general result for Deep GP tails. Duvenaud et al. [31] and Dunlop et al. [27] investigate pathological behaviors that arise with depth, while Agrawal et al. [1] note that “bottlenecked” Deep GP have better performance and correlations among predictive tasks. Our work complements these analysis by characterizing the effects of width.

Connections between Deep GP and neural networks. Many researchers have noted connections between neural networks and Deep GP [e.g. 22, 29, 33, 54]. Duvenaud et al. [31] suggest that infinitely-wide neural networks with intermediate bottleneck layers are nonparametric Deep GP. Agrawal et al. [1] formalize this connection, but note that not all Deep GP can be constructed from bottlenecked neural networks (see Appx. E). In contrast to these prior works, we avoid reducing Deep GP to neural networks, and instead reduce neural networks to degenerate Deep GP.

2.2 A Covariance Perspective on Gaussian Process Limiting Behavior

To decouple the effects of increasing width and capacity, we first prove a new result about GP limits for a more general class of models, including Deep GP as well as typical neural networks. This result forms a necessary foundation for the subsequent theorems that are one main contribution of this work. To begin, note that the proof technique introduced by Neal [62] and extended by others [35, 44, 49, 57, 64, 80] relies on the multivariate central limit theorem, which requires a model with additive structure. Deep GP do not generally decompose in an additive manner, so we establish a more general proof technique. For simplicity, we first present it in the context of neural networks, and then extend it to a more general class of models.

Consider the 2-layer neural network $f_2(\mathbf{f}_1(\mathbf{x}))$, with $\mathbf{f}_1 : \mathbb{R}^D \rightarrow \mathbb{R}^{H_1}$ and $f_2 : \mathbb{R}^{H_1} \rightarrow \mathbb{R}$:

$$\mathbf{f}_1(\cdot) = \mathbf{W}_1^\top(\cdot) + \beta \mathbf{b}_1, \quad f_2(\cdot) = \frac{1}{\sqrt{H_1}} \mathbf{w}_2^\top \sigma(\cdot) + \beta b_2. \quad (1)$$

$\sigma(\cdot)$ is an elementwise nonlinearity, β is a positive constant, and \mathbf{W}_1 , \mathbf{b}_1 , \mathbf{w}_2 , and b_2 are i.i.d. Normal. With randomly initialized parameters, $f_2(\mathbf{f}_1(\cdot)) : \mathbb{R}^D \rightarrow \mathbb{R}$ is a prior distribution over functions, and this distribution converges to a GP in the infinite width limit [62].

Lemma 1. *The neural network defined in Eq. (1) is a Gaussian process if and only if—for any finite set of inputs $\mathbf{X} = [\mathbf{x}_1, \dots, \mathbf{x}_N]$ —the conditional prior covariance $\mathbb{E}_{\mathbf{f}_2|\mathbf{X}, \mathbf{W}_1, \mathbf{b}_1} [\mathbf{f}_2 \mathbf{f}_2^\top]$ is almost surely equal to the marginal prior covariance $\mathbb{E}_{\mathbf{f}_2|\mathbf{X}} [\mathbf{f}_2 \mathbf{f}_2^\top]$, where $\mathbf{f}_2 \mid \mathbf{X} \triangleq [f_2(\mathbf{f}_1(\mathbf{x}_1)), \dots, f_2(\mathbf{f}_1(\mathbf{x}_N))]$.*

Proof. By definition, $f_2(\mathbf{f}_1(\cdot))$ is a GP if and only if $\mathbf{f}_2 \mid \mathbf{X}$ is multivariate Gaussian for any \mathbf{X} . From Eq. (1), we have $p(\mathbf{f}_2 \mid \mathbf{X}, \mathbf{W}_1, \mathbf{b}_1) = \mathcal{N}(\mathbf{0}, \mathbf{K}_{\mathbf{W}_1, \mathbf{b}_1}(\mathbf{X}, \mathbf{X}))$, where $[\mathbf{K}_{\mathbf{W}_1, \mathbf{b}_1}(\mathbf{X}, \mathbf{X})]_{ij} = \beta^2 + \frac{1}{H_1} \sigma(\mathbf{W}_1^\top \mathbf{x}_i + \beta \mathbf{b}_1)^\top \sigma(\mathbf{W}_1^\top \mathbf{x}_j + \beta \mathbf{b}_1)$ ($\mathbf{K}_{\mathbf{W}_1, \mathbf{b}_1}(\mathbf{X}, \mathbf{X})$ is the appropriate kernel Gram matrix). Using Jensen’s inequality, we have a lower bound on the characteristic function of $\mathbf{f}_2 \mid \mathbf{X}$:

$$\begin{aligned} \mathbb{E}_{\mathbf{f}_2|\mathbf{X}} [\exp(i\mathbf{t}^\top \mathbf{f}_2)] &= \mathbb{E}_{\mathbf{W}_1, \mathbf{b}_1} \left[\mathbb{E}_{\mathbf{f}_2|\mathbf{X}, \mathbf{W}_1, \mathbf{b}_1} [\exp(i\mathbf{t}^\top \mathbf{f}_2)] \right] && \text{(law of total expectation)} \\ &= \mathbb{E}_{\mathbf{W}_1, \mathbf{b}_1} \left[\exp\left(-\frac{1}{2}\mathbf{t}^\top \mathbf{K}_{\mathbf{W}_1, \mathbf{b}_1}(\mathbf{X}, \mathbf{X})\mathbf{t}\right) \right] && \text{(char. func. of a Gaussian)} \\ &\geq \exp\left(-\frac{1}{2}\mathbf{t}^\top \mathbb{E}_{\mathbf{W}_1, \mathbf{b}_1} [\mathbf{K}_{\mathbf{W}_1, \mathbf{b}_1}(\mathbf{X}, \mathbf{X})]\mathbf{t}\right). && \text{(convexity of exp)} \end{aligned}$$

This lower bound happens to be the characteristic function of $\mathcal{N}(\mathbf{0}, \mathbb{E}_{\mathbf{W}_1, \mathbf{b}_1} [\mathbf{K}_{\mathbf{W}_1, \mathbf{b}_1}(\mathbf{X}, \mathbf{X})])$. Since \exp is strictly convex, the characteristic function of $\mathbf{f}_2 \mid \mathbf{X}$ equals the Gaussian lower bound $\forall \mathbf{t}$ if and only if $p(\mathbf{K}_{\mathbf{W}_1, \mathbf{b}_1}(\mathbf{X}, \mathbf{X}) \mid \mathbf{W}_1, \mathbf{b}_1) = \mathbb{E}_{\mathbf{f}_2|\mathbf{X}, \mathbf{W}_1, \mathbf{b}_1} [\mathbf{f}_2 \mathbf{f}_2^\top]$ is a constant with probability 1. \square

Seeing that $\frac{1}{H_1} \sigma(\mathbf{W}_1^\top \mathbf{x}_i + \beta \mathbf{b}_1)^\top \sigma(\mathbf{W}_1^\top \mathbf{x}_j + \beta \mathbf{b}_1)$ becomes a.s. constant as $H_1 \rightarrow \infty$, Lemma 1 re-establishes the result of Neal [62] (see Appx. E.1). Critically, unlike Neal’s proof, Lemma 1 neither relies on the central limit theorem nor requires $f_2(\mathbf{f}_1(\cdot))$ to be a neural network; it holds if $p(\mathbf{f}_2 \mid \mathbf{f}_1(\mathbf{x}_1), \dots, \mathbf{f}_1(\mathbf{x}_N))$ is Gaussian. Therefore, we can generalize it to a larger class of models:

Lemma 2. *Let $f_2(\mathbf{f}_1(\cdot)) : \mathbb{R}^D \rightarrow \mathbb{R}$ be a hierarchical model where $f_2(\cdot) : \mathbb{R}^{H_1} \rightarrow \mathbb{R}$ is a GP and $\mathbf{f}_1(\cdot) : \mathbb{R}^D \rightarrow \mathbb{R}^{H_1}$ is a random vector-valued function (including a multilayer hierarchical model). Then $f_2(\mathbf{f}_1(\cdot))$ is a GP if and only if $\mathbb{E}_{\mathbf{f}_2|\mathbf{X}, \mathbf{f}_1(\cdot)} [\mathbf{f}_2 \mathbf{f}_2^\top] = \mathbb{E}_{\mathbf{f}_2|\mathbf{X}} [\mathbf{f}_2 \mathbf{f}_2^\top]$ a.s. for all $\mathbf{X} = [\mathbf{x}_1, \dots, \mathbf{x}_N]$.*

The covariance perspective from Lemmas 1 and 2 is revealing about GP limits. As $\mathbb{E}_{\mathbf{f}_2|\mathbf{X}, \mathbf{f}_1(\cdot)} [\mathbf{f}_2 \mathbf{f}_2^\top]$ converges to $\mathbb{E}_{\mathbf{f}_2|\mathbf{X}} [\mathbf{f}_2 \mathbf{f}_2^\top]$ the model output becomes less and less dependent on $\mathbf{f}_1(\cdot)$. In other words, $f_2(\mathbf{f}_1(\cdot))$ loses its hierarchical nature. We reiterate that Lemma 2 has no requirements about $f_2(\mathbf{f}_1(\cdot))$ transitioning from a finite to infinite basis, nor does it require $f_2(\mathbf{f}_1(\cdot))$ to have additive structure. We demonstrate its generality in the next section with surprising—and troubling—implications.

3 Deep Gaussian Processes Collapse to Shallow Gaussian Processes

Deep GP [17, 24, 25, 72] are hierarchical models where layers $\mathbf{f}_1(\cdot) \dots \mathbf{f}_L(\cdot)$ are (vector-valued) GP:

$$\text{DGP}(\mathbf{x}) = f_L \circ \dots \circ \mathbf{f}_1(\mathbf{x}), \quad \mathbf{f}_i(\cdot) = [f_i^{(1)}(\cdot), \dots, f_i^{(H_i)}(\cdot)], \quad f_i^{(j)}(\cdot) \stackrel{\text{i.i.d.}}{\sim} \mathcal{GP}[0, k_i(\cdot, \cdot)]. \quad (2)$$

H_i is the width of the i^{th} GP, and the output dimensions of each $\mathbf{f}_i(\cdot)$ are independent. By using GP as the primary hierarchical building blocks, Deep GP are generally nonparametric and, assuming the GP layers use universal kernels [59], have infinite representational capacity (see Appx. B.1).

Deep GP versus GP. Deep GP seek to offer more expressivity: conventional single-layer GP—though also nonparametric—are inherently limited by the choice of the prior covariance function [17, 72]. For example, a GP with a RBF covariance is not suitable for data with discontinuities or sharp changes. However, stacking two RBF GP together— $f_2(\mathbf{f}_1(\cdot))$ —can overcome this limitation, since $\mathbf{f}_1(\mathbf{x})$ can encode a warping of \mathbf{x} that “smoothes” the input data for $f_2(\cdot)$ (as we will show in Fig. 1). Empirically, Deep GP have been shown to offer much more accurate predictive posteriors than standard GP [e.g. 16, 22, 24, 25, 28, 41, 72].

Deep GP versus neural networks. (Bayesian) feed-forward neural networks are a strict subclass of Deep GP, albeit a degenerate one [2, 54, 65]. The first neural network layer is a GP with a linear kernel, while subsequent layers are GP with the kernel $k(\mathbf{z}, \mathbf{z}') = \beta^2 + \frac{1}{H_{i-1}} \sum_{i=1}^{H_{i-1}} \sigma(z_i) \sigma(z'_i)$. A neural network, unlike other Deep GP, does not have infinite capacity. Put loosely, a single neural network hidden unit corresponds to a single basis, while in general a single Deep GP unit corresponds to a potentially-infinite basis. See [1, 2, 22, 29, 31, 65] and Appx. B.2 for more discussion on this connection. The critical takeaway is that all of our Deep GP results apply to neural networks as well.

3.1 Wide Deep GP are Gaussian Processes

Having established a model where width does not effect capacity, we now establish what remaining effects width has. Empirical evidence suggests that the choice of width impacts Deep GP predictions [17, 41]. In practice it is common to make Deep GP as wide as comparably-sized neural networks; Salimbeni and Deisenroth [72] for example train Deep GP with ≥ 30 units per layer.

Surprisingly, here we prove that—in the limit of infinite width—Deep GP collapse to single-layer Gaussian processes. Our proof relies on the conditional covariance analysis of the previous section. If the GP layers have non-pathological covariance functions¹—the Deep GP conditional covariance becomes almost surely constant with width (see Lemma 3, Appx. E). Combining this with Lemma 2:

Theorem 1. *Let $f_L \circ \dots \circ \mathbf{f}_1(\mathbf{x})$ be a zero-mean Deep GP (Eq. 2), where each layer satisfies Assumptions 1 and 2 (non-pathological prior covariances that scale with dimensionality—see Appx. E.3). Then $\lim_{H_L \rightarrow \infty} \dots \lim_{H_1 \rightarrow \infty} f_L \circ \dots \circ \mathbf{f}_1(\mathbf{x})$ converges in distribution to a (single-layer) GP.*

(See Appx. E for proof.) The implications of Thm. 1 are paradoxical and unsettling. Deep GP are motivated as a more powerful model than standard GP. However, as we make the model wider, we arrive back where we started—a Gaussian process (although one with a different prior covariance).

A neural network gains representational power in its GP limit, transitioning from a finite-basis model to a nonparametric model. The Deep GP limit on the other hand has no additional representational power, since Deep GP are already universal approximators at any width. (Indeed this fact motivates their use as a control.) The only difference between finite and infinite width Deep GP is the prior distribution itself: transitioning from non-Gaussian to Gaussian with increasing width. In the next section, we investigate how this transition affects model performance.

¹ Any textbook kernel (isotropic kernels, dot product kernels, etc.) or any covariance function with a Fourier-Steiljes representation is “non-pathological;” see Appx. E.3 for formal assumptions.

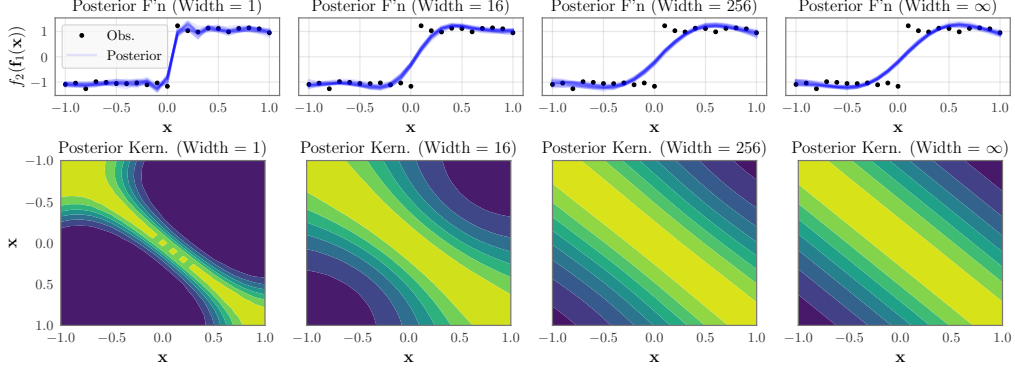


Figure 1: **Top:** Posterior of 2-layer RBF Deep GP fit to a noisy step function. A width-1 Deep GP fits the discontinuity at $\mathbf{x} = 0$. As with increases, the Deep GP converges to a GP with a stationary covariance unable to fit the step. **Bottom:** Average posterior covariance $\mathbb{E}_{\mathbf{f}_1(\mathbf{x}), \mathbf{f}_1(\mathbf{x}')|\mathbf{y}} [k_2(\mathbf{f}_1(\mathbf{x}), \mathbf{f}_1(\mathbf{x}'))]$. The width-1 posterior covariance is non-stationary, with little covariance around $\mathbf{x} = 0$. As width increases, the posterior covariance becomes stationary (as seen by the kernel’s constant diagonals).

4 Large Width Limits the Adaptability of Hierarchical Posteriors

Even with Thm. 1 and its troubling suggestions, it is not immediately clear exactly what is lost in the infinite-width limit. Here, we quantify specific differences in the predictive capabilities of narrow versus wide models. In particular, we analyze Deep GP/neural network posterior distributions, rather than focusing on a single model trained through optimization. We show that these posteriors correspond to a mixture of *data-dependent adaptable bases*; however, as width increases this mixture collapses to the (data-independent) basis of the limiting GP. This result formalizes the often vague notion of *feature learning*, and demonstrates that it is indeed lost in kernel limits.

Hierarchical posteriors correspond to a data-adaptable bases. Consider the (finite-width) 2-layer Deep GP $f_2(f_1(\cdot))$, where $k_1(\cdot, \cdot)$ and $k_2(\cdot, \cdot)$ are the covariance functions of $\mathbf{f}_1(\cdot)$ and $f_2(\cdot)$. Given training data \mathbf{X}, \mathbf{y} , define $\mathbf{F}_1 \triangleq [\mathbf{f}_1(\mathbf{x}_1), \dots, \mathbf{f}_1(\mathbf{x}_N)]$ and $\mathbf{f}_2 \triangleq [f_2(\mathbf{f}_1(\mathbf{x}_1)), \dots, f_2(\mathbf{f}_1(\mathbf{x}_N))]$. Let \mathbf{x}^* be a test input, and let \mathbf{f}_1^* and \mathbf{f}_2^* equal $\mathbf{f}_1(\mathbf{x}^*)$ and $f_2(\mathbf{f}_1(\mathbf{x}^*))$ (see Fig. 5 in Appx. B.3 for a graphical model). Crucially, \mathbf{f}_2 and \mathbf{f}_2^* only depend on \mathbf{F}_1 and \mathbf{f}_1^* through the covariances $\mathbf{K}_2(\mathbf{F}_1, \mathbf{F}_1)$, $\mathbf{k}_2(\mathbf{F}_1, \mathbf{f}_1^*)$, and $k_2(\mathbf{f}_1^*, \mathbf{f}_1^*)$ (which we abbreviate as \mathbf{K}_2 , \mathbf{k}_2^* , and k_2^{**}):

$$p(\mathbf{f}_2 | \mathbf{K}_2) \sim \mathcal{N}(\mathbf{0}, \mathbf{K}_2), \quad p(\mathbf{f}_2^* | k_2^{**}, \mathbf{k}_2^*, \mathbf{K}_2, \mathbf{f}_2) \sim \mathcal{N}(\mathbf{k}_2^{*\top} \mathbf{K}_2^{-1} \mathbf{f}_2, k_2^{**} - \mathbf{k}_2^{*\top} \mathbf{K}_2^{-1} \mathbf{k}_2^*),$$

By D-separation [e.g. 15, Ch. 8], we can factorize the posterior distribution as:

$$p(f_2^*, \mathbf{f}_2, \mathbf{K}_2, \mathbf{k}_2^*, k_2^{**} | \mathbf{y}) = p(f_2^* | \mathbf{f}_2, \mathbf{K}_2, \mathbf{k}_2^*, k_2^{**}) p(\mathbf{f}_2 | \mathbf{K}_2, \mathbf{y}) p(\mathbf{K}_2, \mathbf{k}_2^*, k_2^{**} | \mathbf{y}). \quad (3)$$

See derivation in Appx. B.3. Applying the factorization in Eq. (3), the posterior mean is:

$$\mathbb{E}_{f_2^* | \mathbf{y}} [f_2^*] = \mathbb{E}_{\mathbf{K}_2, \mathbf{k}_2^* | \mathbf{y}} \left[\mathbb{E}_{\mathbf{f}_2 | \mathbf{K}_2, \mathbf{y}} [\mathbf{k}_2^{*\top} \mathbf{K}_2^{-1} \mathbf{f}_2] \right] = \mathbb{E}_{\mathbf{K}_2, \mathbf{k}_2^* | \mathbf{y}} \left[\mathbf{k}_2^{*\top} \mathbf{K}_2^{-1} \mathbb{E}_{\mathbf{f}_2 | \mathbf{K}_2, \mathbf{y}} [\mathbf{f}_2] \right] \quad (4)$$

$$= \mathbb{E}_{\mathbf{f}_1(\mathbf{x}^*), \mathbf{f}_1(\mathbf{x}_1), \dots, \mathbf{f}_1(\mathbf{x}_N) | \mathbf{y}} \left[\sum_{i=1}^N \alpha_i k_2(\mathbf{f}_1(\mathbf{x}_i), \mathbf{f}_1(\mathbf{x}^*)) \right], \quad (5)$$

where the second line follows from \mathbf{K}_2 and \mathbf{k}_2^* being deterministic given $\mathbf{f}_1(\mathbf{x}^*)$, $\mathbf{f}_1(\mathbf{x}_1), \dots, \mathbf{f}_1(\mathbf{x}_N)$. The term inside the Eq. (5) expectation is a function from the reproducing kernel Hilbert space (RKHS) defined by $k_2(\mathbf{f}_1(\cdot), \mathbf{f}_1(\cdot))$. We can thus interpret this expectation as an infinite mixture of functions from different Hilbert spaces. Because the mixture distribution $p(\mathbf{f}_1(\mathbf{x}^*), \mathbf{f}_1(\mathbf{x}_1), \dots, \mathbf{f}_1(\mathbf{x}_N) | \mathbf{y})$ depends on \mathbf{y} , Eq. (5) is an *adaptive data-dependent mixture of RKHS*.

Adaptability is lost in the Gaussian process limit. Recall from Lemma 2 that the conditional prior covariance becomes deterministic as $f_2(\mathbf{f}_1(\cdot))$ converges to a GP. In other words, the prior and posterior distributions over \mathbf{K}_2 and \mathbf{k}_2^* become atomic: $p(\mathbf{K}_2, \mathbf{k}_2^* | \mathbf{y}) = p(\mathbf{K}_{\lim}, \mathbf{k}_{\lim}^* | \mathbf{y}) = \delta[\mathbf{K}_{\lim}, \mathbf{k}_{\lim}^*]$, where \mathbf{K}_{\lim} and \mathbf{k}_{\lim}^* are shorthand for $\mathbb{E}[\mathbf{f}_2 \mathbf{f}_2^\top]$ and $\mathbb{E}[\mathbf{f}_2 f_2^*]$ respectively. Eq. (4) thus collapses to:

$$\lim_{H_1 \rightarrow \infty} \mathbb{E}_{f_2^* | \mathbf{y}} [f_2^*] = \mathbb{E}_{\delta[\mathbf{K}_{\lim}, \mathbf{k}_{\lim}^*]} [\mathbf{k}_2^{*\top} \boldsymbol{\alpha}] = \sum_{i=1}^N \alpha_i k_{\lim}(\mathbf{x}_i, \mathbf{x}^*), \quad (6)$$

which is no longer a mixture of functions from different RKHS. It is instead a function from a single RKHS (that of the limiting GP prior). In other words, while Deep GP (and neural networks) perform *kernel learning (or feature learning)* to adapt to training data, this ability is lost with large width.

Example. Consider a Deep GP with RBF covariances $k_1(\mathbf{x}, \mathbf{x}') = \exp(-\|\mathbf{x} - \mathbf{x}'\|^2/(2D))$ and $k_2(\mathbf{f}_1(\mathbf{x}), \mathbf{f}_1(\mathbf{x}')) = \exp(-\|\mathbf{f}_1(\mathbf{x}) - \mathbf{f}_1(\mathbf{x}')\|^2/(2H_1))$. As we show in Appx. G, this Deep GP converges to a GP with $k_{\lim}(\mathbf{x}, \mathbf{x}') = \exp(\exp(-\|\mathbf{x} - \mathbf{x}'\|^2/(2D)) - 1)$. Note that this limiting covariance is *stationary* and is ill-equipped to model the data step in Fig. 1. However, because $\mathbf{f}_1(\cdot)$ is nonlinear, $k_2(\mathbf{f}_1(\mathbf{x}), \mathbf{f}_1(\mathbf{x}'))$ is *nonstationary*. Fig. 1 (top left) shows that the width-1 Deep GP posterior accurately models both this data. The posterior covariance $\mathbb{E}_{\mathbf{f}_1(\mathbf{x}), \mathbf{f}_1(\mathbf{x}') \mid \mathbf{y}} [k_2(\mathbf{f}_1(\mathbf{x}), \mathbf{f}_1(\mathbf{x}'))]$ (bottom left) features long-range correlations near $\mathbf{x} = \pm 1$ and short-range correlations near $\mathbf{x} = 0$. As width increases, we lose this nonstationarity and the posterior becomes a worse fit.

5 The Difference Between Width and Depth: A Tail Analysis

Our work so far has troubling implications for large width. On the other hand, empirical evidence has shown that depth improves Deep GP performance—as it does for neural nets [e.g. 41, 65, 72] (though pathologies can emerge [27, 31]). Through a novel tail analysis, we show that width makes Deep GP priors more Gaussian, while depth makes them less Gaussian. In other words, *width and depth have opposite effects on Deep GP tails*, results that again also apply to typical neural networks.

Deep GP/neural networks are sharply peaked and heavy tailed. The proof technique used in Lemma 1 can be used to similarly bound the moment generating function of Deep GP marginals:

$$\mathbb{E}_{\mathbf{f}_2} [e^{\mathbf{t}^\top \mathbf{f}_2}] = \mathbb{E}_{\mathbf{F}_1} \left[\mathbb{E}_{\mathbf{f}_2 \mid \mathbf{F}_1} [e^{\mathbf{t}^\top \mathbf{f}_2}] \right] \geq \exp \left(\frac{1}{2} \mathbf{t}^\top \mathbb{E}_{\mathbf{F}_1} [\mathbf{K}_2(\mathbf{F}_1, \mathbf{F}_1)] \mathbf{t} \right) = \mathbb{E}_{\mathbf{g} \sim \mathcal{N}(\mathbf{0}, \mathbf{K}_{\lim})} [e^{\mathbf{t}^\top \mathbf{g}}], \quad (7)$$

where $\mathbf{K}_{\lim} = \mathbb{E}_{\mathbf{f}_2} [\mathbf{f}_2 \mathbf{f}_2^\top] = \mathbb{E}_{\mathbf{F}_1} [\mathbf{K}_2(\mathbf{F}_1, \mathbf{F}_1)]$. Generalizing these bounds to deeper models, we have:

Theorem 2. Let $f_L \circ \dots \circ f_1(\cdot)$ be a zero-mean Deep GP. Given a finite set of inputs $\mathbf{X} = [\mathbf{x}_1, \dots, \mathbf{x}_N]$, define $\mathbf{f}_\ell = [(f_\ell \circ \dots \circ f_1(\mathbf{x}_1)), \dots, (f_\ell \circ \dots \circ f_1(\mathbf{x}_N))]$ for $\ell \in [1, L]$, and define $\mathbf{K}_{\lim} = \mathbb{E}_{\mathbf{f}_L} [\mathbf{f}_L \mathbf{f}_L^\top]$. If $\mathbb{E}_{\mathbf{f}_\ell \mid \mathbf{f}_{\ell-1}} [\mathbf{f}_\ell \mathbf{f}_\ell^\top]$ is not constant a.s. for any $\ell \in [2, L]$, then, $p(\mathbf{f}_L = \mathbf{0}) > \mathcal{N}(\mathbf{g} = \mathbf{0}; \mathbf{0}, \mathbf{K}_{\lim})$.

Theorem 3. Let $\mathbf{t} \in \mathbb{R}^N$. Using the same setup, notation, and assumptions as Thm. 2, the odd moments of $\mathbf{t}^\top \mathbf{f}_L$ are zero and the even moments larger than 2 are super-Gaussian, i.e. $\mathbb{E}_{\mathbf{f}_L} [(\mathbf{t}^\top \mathbf{f}_L)^r] \geq \mathbb{E}_{\mathbf{g} \sim \mathcal{N}(\mathbf{0}, \mathbf{K}_{\lim})} [(\mathbf{t}^\top \mathbf{g})^r]$ for all even $r \geq 4$. Moreover, if $k_L(\cdot, \cdot)$ is bounded almost everywhere, the moment generating function $\mathbb{E}_{\mathbf{f}_L} [\exp(\mathbf{t}^\top \mathbf{f}_L)]$ exists and is similarly super-Gaussian.

(See Appx. F for proofs.) Thm. 2 states that Deep GP marginals are more sharply peaked than a moment-matched Gaussian, while Thm. 3 states that they are also more heavy tailed.

Increasing depth leads to sharper peaks and heavier tails. To understand how depth affects this tail behavior, we examine the Jensen gap in Eq. (7). Consider a 3-layer Deep GP $f_3(\mathbf{f}_2(\mathbf{f}_1(\cdot)))$. If we extend Eq. (7) to 3-layer models, we see that the Jensen gap cascades:

$$\mathbb{E}_{\mathbf{F}_1} \left[\mathbb{E}_{\mathbf{F}_2 \mid \mathbf{F}_1} \left[\exp \left(\frac{1}{2} \mathbf{t}^\top \mathbf{K}_3 \mathbf{t} \right) \right] \right] \geq \mathbb{E}_{\mathbf{F}_1} \left[\exp \left(\frac{1}{2} \mathbf{t}^\top \mathbb{E}_{\mathbf{F}_2 \mid \mathbf{F}_1} [\mathbf{K}_3] \mathbf{t} \right) \right] \geq \exp \left(\frac{1}{2} \mathbf{t}^\top \mathbb{E}_{\mathbf{F}_1} \left[\mathbb{E}_{\mathbf{F}_2 \mid \mathbf{F}_1} [\mathbf{K}_3] \right] \mathbf{t} \right),$$

MGF of 3-layer Deep GP marginal MGF of 2-layer Deep GP marginal MGF of $\mathcal{N}(\mathbf{0}, \mathbb{E}_{\mathbf{F}_1} [\mathbb{E}_{\mathbf{F}_2 \mid \mathbf{F}_1} [\mathbf{K}_3]])$

where \mathbf{K}_3 is short for $\mathbf{K}_3(\mathbf{F}_2(\mathbf{F}_1(\mathbf{X})), \mathbf{F}_2(\mathbf{F}_1(\mathbf{X})))$. The middle term is the moment generating function of a 2-layer Deep GP marginal (where the second layer has covariance $\mathbb{E}_{\mathbf{f}_2(\cdot)} [k_3(\mathbf{f}_2(\cdot), \mathbf{f}_2(\cdot))]$). The right-most term is the moment generating function of a (single-layer) Gaussian. Generalizing this cascade, we see that deeper models are more heavy-tailed. A similar analysis on the characteristic function shows that the peak at the prior mean also becomes sharper with depth (see Appx. F).

Adding additional layers to a Deep GP will change the model’s prior covariance, and thus the effects of depth cannot solely be explained by a tail analysis [27, 31]. Nevertheless, if we control for this change in covariance, we indeed see that depth leads to heavier tails. In Fig. 2 we compare 2-layer and 3-layer Deep GP. The 3-layer models use GP layers with additively-decomposing RBF covariances, while the 2-layer models use layers constructed to match the 3-layer models’ prior covariance (see Appx. H for construction details). The $N = 2$ marginal densities for the 3-layer models (bottom row) are more stretched than the 2-layer densities (top row). We further confirm these effects in Appx. D.

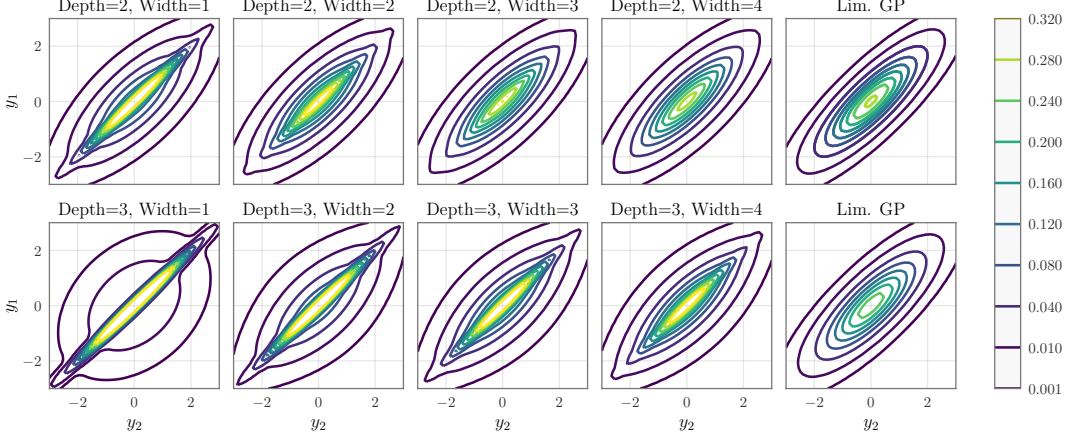


Figure 2: Marginal density $p(y_1, y_2 | \mathbf{x}_1, \mathbf{x}_2)$ for zero-mean Deep GP of various depths and widths on the $N = 2$ dataset $\mathbf{x}_1 = -0.5, \mathbf{x}_2 = 0.5$. All 2-layer models have the same second moments (covariance is that of the 3-layer width-1 RBF-RBF-RBF Deep GP). **Left to right:** width increases, the marginal becomes increasingly Gaussian, tails become thinner, and the peak at $[y_1, y_2] = \mathbf{0}$ loses density. **Top to bottom:** depth increases, tails become fatter, and the peak becomes sharper.

Increasing width leads to flatter peaks and Gaussian tails. Conversely, consider what happens when we make the model wider. We define the sequence of increasingly wide 2-layer Deep GP:

$$\left\{ \text{DGP}^{(m)}(\cdot) \triangleq \frac{1}{\sqrt{m}} \sum_{i=1}^m f_2^{(i)}(f_1^{(i)}(\cdot)) \right\}, \quad \begin{aligned} f_1^{(i)}(\cdot) &\stackrel{\text{i.i.d.}}{\sim} \mathcal{GP}[0, k_1(\cdot, \cdot)], \\ f_2^{(i)}(\cdot) &\stackrel{\text{i.i.d.}}{\sim} \mathcal{GP}[0, k_2(\cdot, \cdot)]. \end{aligned} \quad (8)$$

$\text{DGP}^{(m)}(\cdot)$ is a width- m Deep GP, where the second layer decomposes additively over the m dimensions. By linearity of expectation, each model in the sequence shares the same prior covariance: $\mathbb{E}[\text{DGP}^{(1)}(\mathbf{x}) \text{DGP}^{(1)}(\mathbf{x}')] = \mathbb{E}[\text{DGP}^{(2)}(\mathbf{x}) \text{DGP}^{(2)}(\mathbf{x}')] = \dots \triangleq k_{\text{lim}}(\mathbf{x}, \mathbf{x}')$. Though each model has the same marginal covariance, the *conditional* covariance $\mathbb{E}_{\mathbf{f}_2 \mid \mathbf{f}_1} [\mathbf{f}_2 \mathbf{f}_2^\top] = \frac{1}{m} \sum_{i=1}^m \mathbf{K}_2(\mathbf{f}_1^{(i)}, \mathbf{f}_1^{(i)})$ becomes increasingly concentrated around $\mathbf{K}_{\text{lim}}(\mathbf{X}, \mathbf{X})$ as m increases. This consequentially shrinks the Jensen gap in Eq. (7), and so the Deep GP marginals become increasingly Gaussian. We again visualize this effect in Fig. 2, which depicts marginal densities from 2-layer and 3-layer Deep GP of various width (see Appx. H for details). Compared with the limiting GP (right), the width-1 densities (left) appear sharper near $[0, 0]$ and more stretched at the tails. As width increases, the peaks and tails look increasingly Gaussian (see also Fig. 7 in Appx. D). In this sense, width has the opposite effect as depth—deeper marginals are less Gaussian, while wider marginals are more Gaussian.

6 Experiments

6.1 Regression with Deep GP and Bayesian Neural Networks

To isolate the effects of width and depth, each experiment compares Deep GP/Bayesian neural networks that share the same first and second prior moments, and the Deep GP models use GP layers with universal kernels. To remove any potential side effects from approximate inference methods, we sample Deep GP/neural network posteriors using NUTS [43] and do not use any stochastic inducing point [41, 72] or finite basis [22] approximations. This inference is costly and scales cubically with N ; therefore, we subsample all training datasets to $N \leq 1000$. See Appx. H for experimental details.

Effect of width. We compare 2-layer Deep GP of various width on 6 regression datasets from the UCI dataset repository [9] (see Appx. D for 3-layer results). The first GP layers use a RBF kernel for the prior covariance, while the second layers use a sum of one-dimensional RBF covariance functions. We additionally compare against the limiting (single-layer) GP with the same prior covariance (**Lim. GP**). For each dataset, we choose hyperparameters that maximize the Lim. GP log marginal likelihood. In Fig. 3 (top row) we see a near-monotonic performance degradation as width increases. The width-2 optimum may represent the “sweet spot” for Deep GP width, but it may instead be

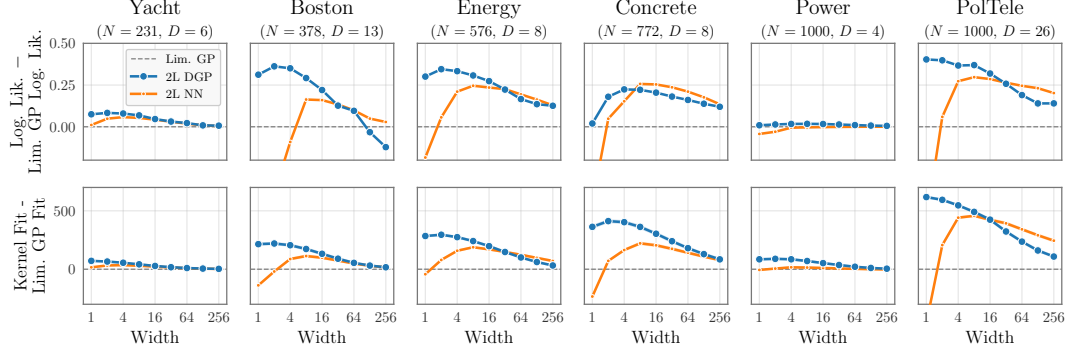


Figure 3: **Top:** Test set log likelihood (LL) of 2-layer Deep GP (and neural networks) regression as a function of width (higher is better). Numbers are shifted so that 0 corresponds to the limiting GP log likelihood. Narrow models achieve the best log likelihood, and performance degrades with width. **Bottom:** Fit of the posterior kernel $k(\mathbf{f}_1(\cdot), \mathbf{f}_1(\cdot))$ on the training data, as measured by Gaussian log marginal likelihood (higher is better). 0 corresponds to the limiting GP log marginal likelihood. Fit becomes increasingly worse with width.

a side-effect of inference difficulties for width-1 models (see Appx. D for a control experiment). Regardless, as our theory predicts, *width is detrimental to Deep GP predictive performance*.

We repeat the experiment for 2-layer neural networks (and 3-layer models in Appx. D), where here the Lim. GP corresponds to the arc-cosine kernel [21, 49]. Fig. 3 indicates an optimal width with regards to test set log likelihood, usually between 8 – 16 hidden units. We expect this optimum exists (and differs from the Deep GP optimum) because narrow models have too few basis functions for these datasets. Thus, after sufficient capacity, *width is harmful to Bayesian neural networks*.

Adaptable versus non-adaptable RKHS. One way to measure the “fit” of a kernel $k(\cdot, \cdot)$ on a regression training dataset \mathbf{X}, \mathbf{y} is the Gaussian log marginal likelihood $\log \mathcal{N}(\mathbf{y}; \mathbf{0}, \mathbf{K}(\mathbf{X}, \mathbf{X}) + \sigma^2 \mathbf{I})$, where σ^2 is an observational noise parameter [e.g. 70]. To demonstrate how Deep GP/neural network posteriors correspond to adaptable RKHS mixtures, the bottom row of Fig. 3 plots the “kernel fit” of $k_2(\mathbf{f}_1(\cdot), \mathbf{f}_1(\cdot))$ for posterior samples of $\mathbf{f}_1(\cdot)$ (see Eq. 5). A higher fit corresponds to a model that is better adapted to the dataset \mathbf{X}, \mathbf{y} . We see that narrower Deep GP almost universally achieve better kernel fit than wider Deep GP, which converge to the same fit as the limiting GP. (Standard deviations, depicted by shaded regions, are generally imperceptible.) Bayesian neural networks achieve best “kernel fit” at 8 – 16 hidden units, and then converge to the limiting Deep GP with further width.

Effect of depth, controlling for covariance. Table 1 displays Deep GP test set log likelihood as a function of depth. Again, we isolate the tail effects of depth by ensuring that all models share the same first and second moments. We construct a GP and a 2-layer Deep GP that match the moments of a width-2 3-layer Deep GP with RBF covariances, and we use hyperparameters that maximize the limiting GP marginal likelihood for each dataset. Note that computing the limiting covariance of ≥ 3 layer models involves intractable integrals that we approximate with quadrature (see Appx. G). Our findings confirm that—in this controlled setting—depth unlike width improves test set performance.

6.2 Standard (Optimized, Non-Bayesian) Neural Networks

Here our goal is to represent “real world” models without a Bayesian treatment, and thus we do not control the prior covariance across models. However, we scale the outputs of layer- ℓ by $1/\sqrt{H_\ell}$ to match the GP-limiting neural net construction in Eq. (1). We choose the L_2 regularization parameter so that it corresponds to a parameter prior of $\mathcal{N}(0, 20)$.² All models are trained without data augmentation. Fig. 4 depicts test set accuracy for increasingly wide models trained on MNIST [48] (left) and CIFAR-10 [47] (right). On MNIST we examine two sequences of 3-layer (non-convolutional) networks: one where the width of both hidden layers increases simultaneously ($H_1 = H_2$), and one where all but the final layer have fixed width ($H_1 = 256$). We test these

²The L_2 parameter equivalent to this prior decreases with N , and—due to the $\sqrt{1/H_\ell}$ scaling—effectively increases with width. The $\mathcal{N}(0, 20)$ prior is equivalent to a weight decay of 10^{-4} for $N = 50000$ and $H_\ell = 100$.

Table 1: Test set log likelihood (LL) of Deep GP regression as a function of depth (higher is better). Depth = 1 refers to the limiting GP. For each dataset, the models are constructed to have the same first and second moments. Unlike width, deeper models generally have better performance.

Depth	Yacht ($N = 231, D = 6$)	Boston ($N = 378, D = 13$)	Energy ($N = 576, D = 8$)	Concrete ($N = 772, D = 8$)	Power ($N = 1000, D = 4$)	PolTele ($N = 1000, D = 26$)
1	-0.532	-0.890	-0.477	-0.663	-0.249	-0.476
2	-0.520	-0.684	-0.434	-0.573	-0.260	-0.381
3	-0.482	-0.609	-0.383	-0.620	-0.251	-0.318

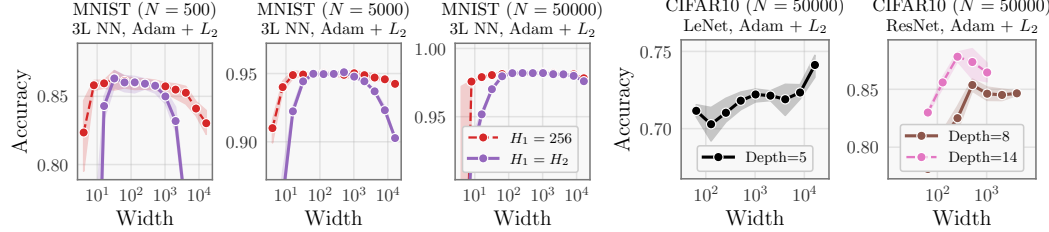


Figure 4: Effect of width on standard (non-Bayesian) neural networks. Shaded regions depict standard error. **Left:** 3-layer feed-forward networks trained on various subsets of MNIST. Test set accuracy is maximized when width ≈ 100 , after which width becomes decremental. **Right:** LeNet and wide ResNets trained on CIFAR-10. The best LeNet has ≥ 16000 hidden units, likely because this model is too shallow for sufficient capacity. For deeper ResNet models, accuracy is best when width ≤ 500 .

sequences on variously-sized subsets of the training data, and observe a maximum test set accuracy for width ≈ 100 networks. On CIFAR-10 we examine 5-layer LeNet models [48] and 8- and 14-layer wide ResNet models [42, 84]. For LeNet, we only vary the width of the fully connected layers, and we observe varied performance behavior with width, possibly indicating LeNet is too shallow for sufficient capacity on this dataset. Indeed, deeper ResNets—where we increase width of all layers simultaneously—achieve best accuracy when width ≤ 500 . These results reiterate that even in typical networks, once sufficient capacity is reached, *large width adversely affects model performance*.

7 Discussion

This paper shows that, across typical neural networks, Deep GP, and Bayesian neural networks, *width is fundamentally detrimental after sufficient capacity is reached*.

Even with that result, we can ask when large width might still be beneficial? Our results assume that layers are conditionally Gaussian, and different priors may have different effects. Researchers have touted benefits of width, both in terms of a more favorable optimization landscape [6, 26, 52, 63, 75] and better generalization through the double descent phenomenon [11, 18, 61]. Moreover, there are (non-Bayesian) infinite-width constructions that avoid the limiting kernel behavior studied in this work [e.g. 20, 39, 58, 82]. We emphasize that our results do not conflict with these prior works, but rather reflect a different perspective. The models we study correspond to a Gaussian prior on parameters. Relaxing this correspondence, for example by changing the weight decay parameter, may lessen the consequences of width that we observe. Nevertheless, our results suggest that the inductive bias of width is harmful, even if these undesirable effects can be avoided via careful construction.

Finally, it is worth considering when one might still choose a conventional shallow GP over a deep model. An often-touted benefit of Gaussian processes is the ability to encode prior domain knowledge via the choice of covariance function. In Appx. C, we prove that certain prior covariances cannot be expressed by adaptable hierarchical models. For example, a Deep GP that is composed of stationary GP layers cannot model anti-correlations a priori (Thm. 4, Appx. C), whereas (single-layer) stationary GP can have positive and negative prior covariances. Nevertheless, Deep GP are capable of modeling many common covariance functions, including the RBF, Matérn, and rational quadratic kernels. In Appx. C we demonstrate a 2-layer Deep GP construction of any width that is capable of producing prior covariances that match most isotropic kernels (Thm. 5, Appx. C). In other words, a Deep GP can match the first and second moments of most GP, while also offering an adaptable posterior.

Acknowledgments and Disclosure of Funding

This work was supported by the Simons Foundation, McKnight Foundation, the Grossman Center, and the Gatsby Charitable Trust.

References

- [1] D. Agrawal, T. Papamarkou, and J. Hinkle. Wide neural networks with bottlenecks are deep Gaussian processes. *Journal of Machine Learning Research*, 21(175):1–66, 2020.
- [2] L. Aitchison. Why bigger is not always better: on finite and infinite neural networks. In *ICML*, 2020.
- [3] Z. Allen-Zhu and Y. Li. What can ResNet learn efficiently, going beyond kernels? In *NeurIPS*, 2019.
- [4] Z. Allen-Zhu and Y. Li. Backward feature correction: How deep learning performs deep learning. *arXiv preprint arXiv:2001.04413*, 2020.
- [5] Z. Allen-Zhu, Y. Li, and Y. Liang. Learning and generalization in overparameterized neural networks, going beyond two layers. In *NeurIPS*, 2019.
- [6] S. Arora, S. Du, W. Hu, Z. Li, and R. Wang. Fine-grained analysis of optimization and generalization for overparameterized two-layer neural networks. In *ICML*, 2019.
- [7] S. Arora, S. S. Du, W. Hu, Z. Li, R. Salakhutdinov, and R. Wang. On exact computation with an infinitely wide neural net. In *NeurIPS*, 2019.
- [8] S. Arora, S. S. Du, Z. Li, R. Salakhutdinov, R. Wang, and D. Yu. Harnessing the power of infinitely wide deep nets on small-data tasks. In *ICLR*, 2020.
- [9] A. Asuncion and D. Newman. Uci machine learning repository, 2007. URL <http://archive.ics.uci.edu/ml/index.php>.
- [10] Y. Bai and J. D. Lee. Beyond linearization: On quadratic and higher-order approximation of wide neural networks. In *ICLR*, 2020.
- [11] M. Belkin, D. Hsu, S. Ma, and S. Mandal. Reconciling modern machine-learning practice and the classical bias–variance trade-off. *Proceedings of the National Academy of Sciences*, 116(32):15849–15854, 2019.
- [12] Y. Bengio, O. Delalleau, and N. Le Roux. The curse of dimensionality for local kernel machines. 2005.
- [13] P. Billingsley. *Convergence of probability measures*. John Wiley & Sons, 2013.
- [14] E. Bingham, J. P. Chen, M. Jankowiak, F. Obermeyer, N. Pradhan, T. Karaletsos, R. Singh, P. Szerlip, P. Horsfall, and N. D. Goodman. Pyro: Deep universal probabilistic programming. *The Journal of Machine Learning Research*, 20(1):973–978, 2019.
- [15] C. M. Bishop. *Pattern recognition and machine learning*. Springer, 2006.
- [16] K. Blomqvist, S. Kaski, and M. Heinonen. Deep convolutional Gaussian processes. In *Joint European Conference on Machine Learning and Knowledge Discovery in Databases*, 2019.
- [17] T. Bui, D. Hernández-Lobato, J. Hernandez-Lobato, Y. Li, and R. Turner. Deep Gaussian processes for regression using approximate expectation propagation. In *ICML*, 2016.
- [18] Y. Cao and Q. Gu. Generalization bounds of stochastic gradient descent for wide and deep neural networks. In *NeurIPS*, 2020.
- [19] M. Chen, Y. Bai, J. D. Lee, T. Zhao, H. Wang, C. Xiong, and R. Socher. Towards understanding hierarchical learning: Benefits of neural representations. In *NeurIPS*, 2020.
- [20] L. Chizat and F. Bach. On the global convergence of gradient descent for over-parameterized models using optimal transport. In *NeurIPS*, 2018.
- [21] Y. Cho and L. Saul. Kernel methods for deep learning. In *NeurIPS*, 2009.
- [22] K. Cutajar, E. V. Bonilla, P. Michiardi, and M. Filippone. Random feature expansions for deep Gaussian processes. In *ICML*, 2017.

[23] Z. Dai, A. C. Damianou, J. González, and N. D. Lawrence. Variational auto-encoded deep Gaussian processes. In *ICLR*, 2016.

[24] A. Damianou. *Deep Gaussian processes and variational propagation of uncertainty*. PhD thesis, University of Sheffield, 2015.

[25] A. Damianou and N. Lawrence. Deep Gaussian processes. In *AISTATS*, 2013.

[26] S. Du, J. Lee, H. Li, L. Wang, and X. Zhai. Gradient descent finds global minima of deep neural networks. In *ICML*, 2019.

[27] M. M. Dunlop, M. A. Girolami, A. M. Stuart, and A. L. Teckentrup. How deep are deep Gaussian processes? *Journal of Machine Learning Research*, 19(54):1–46, 2018.

[28] V. Dutordoir, M. Wilk, A. Artemev, and J. Hensman. Bayesian image classification with deep convolutional Gaussian processes. In *AISTATS*, 2020.

[29] V. Dutordoir, J. Hensman, M. van der Wilk, C. H. Ek, Z. Ghahramani, and N. Durrande. Deep neural networks as point estimates for deep Gaussian processes. *arXiv preprint arXiv:2105.04504*, 2021.

[30] V. Dutordoir, H. Salimbeni, E. Hambro, J. McLeod, F. Leibfried, A. Artemev, M. van der Wilk, J. Hensman, M. P. Deisenroth, and S. John. Gpflux: A library for deep Gaussian processes. *arXiv preprint arXiv:2104.05674*, 2021.

[31] D. Duvenaud, O. Rippel, R. Adams, and Z. Ghahramani. Avoiding pathologies in very deep networks. In *AISTATS*, 2014.

[32] S. Fort, G. K. Dziugaite, M. Paul, S. Kharaghani, D. M. Roy, and S. Ganguli. Deep learning versus kernel learning: an empirical study of loss landscape geometry and the time evolution of the neural tangent kernel. In *NeurIPS*, 2020.

[33] Y. Gal and Z. Ghahramani. Dropout as a Bayesian approximation: Representing model uncertainty in deep learning. In *ICML*, 2016.

[34] J. R. Gardner, G. Pleiss, K. Q. Weinberger, D. Bindel, and A. G. Wilson. GPyTorch: Blackbox matrix-matrix Gaussian process inference with GPU acceleration. In *NeurIPS*, 2018.

[35] A. Garriga-Alonso, C. E. Rasmussen, and L. Aitchison. Deep convolutional networks as shallow Gaussian processes. In *ICLR*, 2019.

[36] M. G. Genton. Classes of kernels for machine learning: a statistics perspective. *Journal of Machine Learning Research*, 2(Dec):299–312, 2001.

[37] B. Ghorbani, S. Mei, T. Misiakiewicz, and A. Montanari. Limitations of lazy training of two-layers neural networks. In *NeurIPS*, 2019.

[38] B. Ghorbani, S. Mei, T. Misiakiewicz, and A. Montanari. When do neural networks outperform kernel methods? In *NeurIPS*, 2020.

[39] E. Golikov. Towards a general theory of infinite-width limits of neural classifiers. In *ICML*, 2020.

[40] I. Goodfellow, Y. Bengio, A. Courville, and Y. Bengio. *Deep learning*. MIT press Cambridge, 2016.

[41] M. Havasi, J. M. Hernández-Lobato, and J. J. Murillo-Fuentes. Inference in deep Gaussian processes using stochastic gradient Hamiltonian Monte Carlo. In *NeurIPS*, 2018.

[42] K. He, X. Zhang, S. Ren, and J. Sun. Deep residual learning for image recognition. In *CVPR*, 2016.

[43] M. D. Hoffman and A. Gelman. The no-u-turn sampler: adaptively setting path lengths in Hamiltonian Monte Carlo. *Journal of Machine Learning Research*, 15(1):1593–1623, 2014.

[44] J. Hron, Y. Bahri, J. Sohl-Dickstein, and R. Novak. Infinite attention: NNGP and NTK for deep attention networks. In *ICML*, 2020.

[45] A. Jacot, F. Gabriel, and C. Hongler. Neural tangent kernel: Convergence and generalization in neural networks. In *NeurIPS*, 2018.

[46] D. P. Kingma and J. Ba. Adam: A method for stochastic optimization. In *ICLR*, 2015.

[47] A. Krizhevsky. Learning multiple layers of features from tiny images. 2009.

[48] Y. LeCun, L. Bottou, Y. Bengio, and P. Haffner. Gradient-based learning applied to document recognition. *Proceedings of the IEEE*, 86(11):2278–2324, 1998.

[49] J. Lee, Y. Bahri, R. Novak, S. S. Schoenholz, J. Pennington, and J. Sohl-Dickstein. Deep neural networks as Gaussian processes. In *ICLR*, 2018.

[50] J. Lee, L. Xiao, S. S. Schoenholz, Y. Bahri, R. Novak, J. Sohl-Dickstein, and J. Pennington. Wide neural networks of any depth evolve as linear models under gradient descent. In *NeurIPS*, 2019.

[51] J. Lee, S. Schoenholz, J. Pennington, B. Adlam, L. Xiao, R. Novak, and J. Sohl-Dickstein. Finite versus infinite neural networks: an empirical study. In *NeurIPS*, 2020.

[52] H. Li, Z. Xu, G. Taylor, C. Studer, and T. Goldstein. Visualizing the loss landscape of neural nets. In *NeurIPS*, 2018.

[53] Y. Li, T. Ma, and H. R. Zhang. Learning over-parametrized two-layer neural networks beyond NTK. In *COLT*, 2020.

[54] C. Louizos and M. Welling. Structured and efficient variational deep learning with matrix Gaussian posteriors. In *ICML*, 2016.

[55] C.-K. Lu, S. C.-H. Yang, X. Hao, and P. Shafto. Interpretable deep Gaussian processes with moments. In *AISTATS*, 2020.

[56] Z. Lu, H. Pu, F. Wang, Z. Hu, and L. Wang. The expressive power of neural networks: A view from the width. In *NeurIPS*, 2017.

[57] A. G. d. G. Matthews, M. Rowland, J. Hron, R. E. Turner, and Z. Ghahramani. Gaussian process behaviour in wide deep neural networks. In *ICLR*, 2018.

[58] S. Mei, A. Montanari, and P.-M. Nguyen. A mean field view of the landscape of two-layer neural networks. *Proceedings of the National Academy of Sciences*, 115(33):E7665–E7671, 2018.

[59] C. A. Micchelli, Y. Xu, and H. Zhang. Universal kernels. *Journal of Machine Learning Research*, 7(12), 2006.

[60] G. Montúfar, R. Pascanu, K. Cho, and Y. Bengio. On the number of linear regions of deep neural networks. In *NeurIPS*, 2014.

[61] P. Nakkiran, G. Kaplun, Y. Bansal, T. Yang, B. Barak, and I. Sutskever. Deep double descent: Where bigger models and more data hurt. In *ICLR*, 2020.

[62] R. M. Neal. *Bayesian learning for neural networks*. PhD thesis, University of Toronto, 1995.

[63] Q. Nguyen and M. Hein. The loss surface of deep and wide neural networks. In *ICML*, 2017.

[64] R. Novak, L. Xiao, J. Lee, Y. Bahri, G. Yang, J. Hron, D. A. Abolafia, J. Pennington, and J. Sohl-Dickstein. Bayesian deep convolutional networks with many channels are Gaussian processes. In *ICLR*, 2019.

[65] S. W. Ober and L. Aitchison. Global inducing point variational posteriors for Bayesian neural networks and deep Gaussian processes. *arXiv preprint arXiv:2005.08140*, 2020.

[66] A. Paszke, S. Gross, F. Massa, A. Lerer, J. Bradbury, G. Chanan, T. Killeen, Z. Lin, N. Gimelshein, L. Antiga, et al. PyTorch: An imperative style, high-performance deep learning library. In *NeurIPS*, 2019.

[67] B. Poole, S. Lahiri, M. Raghu, J. Sohl-Dickstein, and S. Ganguli. Exponential expressivity in deep neural networks through transient chaos. In *NeurIPS*, 2016.

[68] M. Raghu, B. Poole, J. Kleinberg, S. Ganguli, and J. Sohl-Dickstein. On the expressive power of deep neural networks. In *ICML*, 2017.

[69] A. Rahimi, B. Recht, et al. Random features for large-scale kernel machines. In *NeurIPS*, 2007.

[70] C. E. Rasmussen and C. Williams. *Gaussian processes for machine learning*, volume 1. MIT Press, 2006.

[71] A. Romero, N. Ballas, S. E. Kahou, A. Chassang, C. Gatta, and Y. Bengio. Fitnets: Hints for thin deep nets. In *ICLR*, 2015.

[72] H. Salimbeni and M. Deisenroth. Doubly stochastic variational inference for deep Gaussian processes. In *NeurIPS*, 2017.

- [73] I. J. Schoenberg. Metric spaces and completely monotone functions. *Annals of Mathematics*, pages 811–841, 1938.
- [74] V. Shankar, A. Fang, W. Guo, S. Fridovich-Keil, J. Ragan-Kelley, L. Schmidt, and B. Recht. Neural kernels without tangents. In *ICML*, 2020.
- [75] M. Soltanolkotabi, A. Javanmard, and J. D. Lee. Theoretical insights into the optimization landscape of over-parameterized shallow neural networks. *IEEE Transactions on Information Theory*, 65(2):742–769, 2018.
- [76] M. Telgarsky. Benefits of depth in neural networks. In *COLT*, 2016.
- [77] M. Vladimirova, J. Verbeek, P. Mesejo, and J. Arbel. Understanding priors in Bayesian neural networks at the unit level. In *ICML*, 2019.
- [78] Y. Wang, M. Brubaker, B. Chaib-Draa, and R. Urtasun. Sequential inference for deep Gaussian process. In *AISTATS*, 2016.
- [79] A. Yaglom. *Correlation theory of stationary and related random functions*. Springer Series in Statistics, New York, 1987.
- [80] G. Yang. Tensor programs I: Wide feedforward or recurrent neural networks of any architecture are gaussian processes. In *NeurIPS*, 2019.
- [81] G. Yang. Tensor programs II: Neural tangent kernel for any architecture. *arXiv preprint arXiv:2006.14548*, 2020.
- [82] G. Yang and E. J. Hu. Feature learning in infinite-width neural networks. *arXiv preprint arXiv:2011.14522*, 2020.
- [83] G. Yehudai and O. Shamir. On the power and limitations of random features for understanding neural networks. In *NeurIPS*, 2019.
- [84] S. Zagoruyko and N. Komodakis. Wide residual networks. In *BMVC*, 2016.
- [85] J. A. Zavatone-Veth and C. Pehlevan. Exact priors of finite neural networks. *arXiv preprint arXiv:2104.11734*, 2021.

Supplementary Information for: The Limitations of Large Width in Neural Networks: A Deep Gaussian Process Perspective

Geoff Pleiss
Columbia University
gmp2162@columbia.edu

John P. Cunningham
Columbia University
jpc2181@columbia.edu

A Broader Impact

This paper analyzes two existing classes of models: Deep GP and neural networks. We believe that our findings will be of interest to researchers and machine learning practitioners, offering useful guidance for Deep GP and neural network architectures. Because we are neither introducing new algorithms nor introducing new use cases of existing algorithms, we do not foresee any major ethical impacts from this work. However, we do note that this paper primarily focuses on how width affects performance metrics (e.g. accuracy, log likelihood, etc.) and does not focus on other metrics that may be of interest to practitioners and society at large (e.g. interpretability, energy usage, fairness, etc.).

B Deep Gaussian Processes

In this section we discuss various Deep GP facts presented throughout the main paper.

B.1 Capacity of Deep GP

Here we formalize the claim that Deep GP have “infinite capacity.” Standard Gaussian processes are nonparametric, and—if the prior covariance is a universal kernel [59]—then any function (or an arbitrarily precise approximation thereof) is a draw from its prior. A Deep GP composes multiple GP as different layers. If all GP layers use universal kernels for covariance priors, then any (arbitrarily precise approximation of a) function $h(\cdot)$ is a draw from the Deep GP prior. (Draw the identity function from the first $L - 1$ GP layers, and then draw $h(\cdot)$ from the last GP layer.) In this sense, Deep GP as well as standard GP can model any function to arbitrary precision and in this sense have infinite capacity.

B.2 Connection Between Neural Networks and Deep GP

Throughout this paper we note that feed-forward (Bayesian) neural networks are a degenerate subclass of Deep Gaussian processes. We will now formalize this connection, which has also been noted in several previous works [e.g. 2, 54, 65].

To show that the neural network defined in Eq. (1) is a (degenerate) Deep GP, we must show that each of its layers corresponds to a (degenerate, vector-valued) Gaussian process. Recall that a Gaussian process $f(\cdot) \sim \mathcal{GP}$ is a distribution over functions where every finite marginal distribution $\mathbf{f} = [f(\mathbf{x}_1), \dots, f(\mathbf{x}_N)]$ is multivariate Gaussian consistent with some covariance function. The first layer of the Eq. (1) neural network is given by

$$f_1^{(i)}(\mathbf{x}) = \mathbf{w}_1^{(i)\top}(\mathbf{x}) + \beta b_1^{(i)},$$

where the entries of $\mathbf{w}_1^{(i)}$ and $b_1^{(i)}$ are i.i.d. unit Normal. Using standard Gaussian identities, we have that $\mathbf{f}_1^{(i)} = \mathcal{N}(\mathbf{0}, \beta + \mathbf{X}\mathbf{X}^\top)$, where $\mathbf{X} = [\mathbf{x}_1, \dots, \mathbf{x}_N]$. Thus, the first layer corresponds to a

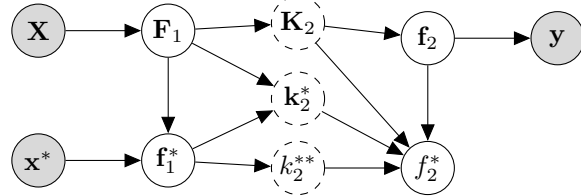


Figure 5: 2-layer Deep GP. \mathbf{X}, \mathbf{y} are the training data; \mathbf{x}^* is some unobserved test input. \mathbf{F}_1 and \mathbf{f}_1^* are the first layer outputs for the training inputs and test input, respectively. \mathbf{f}_2 and \mathbf{f}_2^* are the second layer outputs for the train/test inputs, which only depend on $\mathbf{F}_1, \mathbf{f}_1^*$ through the prior covariance matrices $\mathbf{K}_2 = \mathbf{K}_2(\mathbf{F}_1, \mathbf{F}_1)$, $\mathbf{k}_2^* = \mathbf{k}_2(\mathbf{F}_1, \mathbf{f}_1^*)$, and $\mathbf{k}_2^{**} = \mathbf{k}_2(\mathbf{f}_1^*, \mathbf{f}_1^*)$.

vector-valued Gaussian process with the (degenerate) linear prior covariance. The second layer of the Eq. (1) neural network is given by

$$f_2(\mathbf{z}) = \frac{1}{\sqrt{H_1}} \mathbf{w}_2^\top \boldsymbol{\sigma}(\mathbf{z}) + \beta b_2,$$

where again the entries of \mathbf{w}_2 and b_2 are i.i.d. unit Normal. We have that $\mathbf{f}_2 \mid \mathbf{F}_1 = \mathcal{N}(\mathbf{0}, \beta + \boldsymbol{\sigma}(\mathbf{F}_1)\boldsymbol{\sigma}(\mathbf{F}_1)^\top)$, where $\mathbf{F}_1 = [\mathbf{f}_1(\mathbf{x}_1), \dots, \mathbf{f}_1(\mathbf{x}_N)]$ and $\boldsymbol{\sigma}(\mathbf{F}_1)$ corresponds to the elementwise nonlinearity $\boldsymbol{\sigma}(\cdot)$ applied to each entry of \mathbf{F}_1 . Thus, the second layer also corresponds to a Gaussian process with a degenerate prior covariance.

Neural networks versus Deep GP. While (Bayesian) neural networks meet the definition of a Deep GP, their covariance functions only correspond to a finite basis and therefore they do not have the same properties as nonparametric Deep GP (i.e. the ability to model any function to arbitrary precision). In this sense, it is common to treat neural networks and Deep GP as two separate classes of models with different predictive properties. However, we emphasize that the theoretical results in this paper make no assumptions about whether or not a Deep GP is nonparametric, and therefore the behaviors that we analyze are inherent to both classes of models. In this sense, it is useful for our purposes to group nonparametric Deep GP and neural networks into a single class of models.

B.3 Factorization of Deep GP Posterior

Here we supply additional details for the Sec. 4 derivation of the Deep GP posterior mean. Consider a 2-layer zero-mean Deep-GP $f_2(\mathbf{f}_1(\cdot))$. Fig. 5 depicts the relationships between these variables, using the same notation as in Sec. 4. Now consider the posterior distribution

$$p(f_2^*, \mathbf{f}_2, \mathbf{F}_1, \mathbf{f}_1 \mid \mathbf{y}) = p(f_2^* \mid \mathbf{f}_2, \mathbf{f}_1^*, \mathbf{F}_1, \mathbf{y}) p(\mathbf{f}_2 \mid \mathbf{F}_1, \mathbf{y}, \mathbf{f}_1^*) p(\mathbf{f}_1^*, \mathbf{F}_1 \mid \mathbf{y}),$$

where we have omitted the dependence on \mathbf{X} and \mathbf{x}^* for clarity. Apply the rules of D-separation using Fig. 5, we see that f_2^* only depends on \mathbf{y} through \mathbf{f}_2 , and thus f_2^* is conditionally independent from \mathbf{y} given \mathbf{f}_2 . Furthermore, we see that \mathbf{f}_2 is only connected to \mathbf{f}_1^* through f_2^* , and so \mathbf{f}_2 is conditionally independent from \mathbf{f}_1^* if f_2^* is marginalized out. Thus, we can simplify the posterior factorization to:

$$p(f_2^*, \mathbf{f}_2, \mathbf{F}_1, \mathbf{f}_1 \mid \mathbf{y}) = p(f_2^* \mid \mathbf{f}_2, \mathbf{f}_1^*, \mathbf{F}_1) p(\mathbf{f}_2 \mid \mathbf{F}_1, \mathbf{y}) p(\mathbf{f}_1^*, \mathbf{F}_1 \mid \mathbf{y}), \quad (9)$$

Crucially, \mathbf{f}_2 and f_2^* only depend on \mathbf{F}_1 and \mathbf{f}_1^* through \mathbf{K}_2 , \mathbf{k}_2^* , and \mathbf{k}_2^{**} :

$$p(\mathbf{f}_2 \mid \mathbf{K}_2) \sim \mathcal{N}(\mathbf{0}, \mathbf{K}_2), \quad p(f_2^* \mid \mathbf{k}_2^*, \mathbf{k}_2^*, \mathbf{K}_2, \mathbf{f}_2) \sim \mathcal{N}(\mathbf{k}_2^{*\top} \mathbf{K}_2^{-1} \mathbf{f}_2, \mathbf{k}_2^{**} - \mathbf{k}_2^{*\top} \mathbf{K}_2^{-1} \mathbf{k}_2^*),$$

(If $f_2(\mathbf{f}_1(\cdot))$ is a neural network or any other degenerate Deep GP, the \mathbf{K}_2^{-1} term can be replaced with its pseudoinverse.) This relationship is also depicted graphically in Fig. 5. \mathbf{K}_2 , \mathbf{k}_2^* , and \mathbf{k}_2^{**} are deterministic given \mathbf{F}_1 and \mathbf{f}_1^* , and we do not ultimately care about the values of \mathbf{F}_1 and \mathbf{f}_1^* since they are intermediate latent variables. Therefore, we can rewrite the factorization in Eq. (9) where we replace $\mathbf{F}_1, \mathbf{f}_1^*$ with $\mathbf{K}_2, \mathbf{k}_2^*$, and \mathbf{k}_2^{**} :

$$p(f_2^*, \mathbf{f}_2, \mathbf{K}_2, \mathbf{k}_2^*, \mathbf{k}_2^{**} \mid \mathbf{y}) = p(f_2^* \mid \mathbf{f}_2, \mathbf{K}_2, \mathbf{k}_2^*, \mathbf{k}_2^{**}) p(\mathbf{f}_2 \mid \mathbf{K}_2, \mathbf{y}) p(\mathbf{K}_2, \mathbf{k}_2^*, \mathbf{k}_2^{**} \mid \mathbf{y}). \quad (10)$$

Applying the factorization in Eq. (3), the posterior mean is:

$$\begin{aligned}\mathbb{E}_{f_2^*|y} [f_2^*] &= \mathbb{E}_{\mathbf{K}_2, \mathbf{k}_2^*, k_2^*|y} \left[\mathbb{E}_{f_2|K_2, y} \left[f_2^* | f_2, \mathbf{K}_2, \mathbf{k}_2^*, k_2^* \right] \right] \\ &= \mathbb{E}_{\mathbf{K}_2, \mathbf{k}_2^*|y} \left[\mathbb{E}_{f_2|K_2, y} \left[\mathbf{k}_2^{*\top} \mathbf{K}_2^{-1} \mathbf{f}_2 \right] \right] \\ &= \mathbb{E}_{\mathbf{K}_2, \mathbf{k}_2^*|y} \left[\mathbf{k}_2^{*\top} \overbrace{\mathbf{K}_2^{-1} \mathbb{E}_{f_2|K_2, y} [\mathbf{f}_2]}^{\alpha} \right]\end{aligned}\quad (11)$$

$$= \mathbb{E}_{\mathbf{K}_2, \mathbf{k}_2^*|y} \left[\mathbf{k}_2^{*\top} \mathbf{K}_2^{-1} \mathbb{E}_{f_2|K_2, y} [\mathbf{f}_2] \right] \quad (12)$$

(Again, if $f_2(\mathbf{f}_1(\cdot))$ is a neural network, the \mathbf{K}_2^{-1} term in Eqs. (11) and (12) can be replaced with its pseudoinverse.) Finally, since $\mathbf{K}_2, \mathbf{k}_2^*$ are deterministic transforms of $\mathbf{f}_1(\mathbf{x}^*), \mathbf{f}_1(\mathbf{x}_1), \dots, \mathbf{f}_1(\mathbf{x}_N)$, we can rewrite Eq. (12) as:

$$\mathbb{E}_{f_2^*|y} [f_2^*] = \mathbb{E}_{\mathbf{f}_1(\mathbf{x}^*), \mathbf{f}_1(\mathbf{x}_1), \dots, \mathbf{f}_1(\mathbf{x}_N)|y} \left[\sum_{i=1}^N \alpha_i k_2(\mathbf{f}_1(\mathbf{x}_i), \mathbf{f}_1(\mathbf{x}^*)) \right],$$

which completes the derivation of Eq. (5) in Sec. 4.

C What Prior Covariance Functions can be Modeled by Deep Gaussian Processes?

The functional properties of standard Gaussian processes are largely determined by the choice of prior covariance function [70]. Any positive definite function is a valid GP covariance, making it possible to encode many types of functional priors. For Deep GP, it is reasonable to assume that its prior second moment also has significant influence on its inductive bias and functional properties. To that end, it is of interest to determine what covariances can be modeled by Deep GP a priori.

We present two theoretical results in this section. The first is a negative result (Thm. 4), which states that Deep GP with stationary GP layers can only model non-negative covariance functions a priori. This is in contrast to standard GP, which are capable of expressing anti-correlations with stationary covariance priors. The second is a positive result (Thm. 5), which demonstrates a Deep GP construction capable of modeling most isotropic covariance priors. We note that isotropic functions (e.g. RBF, Matérn, rational quadratic, etc.) are some of the most common covariance priors.

Theorem 4. *Let $DGP(\cdot) = f_L \circ \dots \circ f_1(\cdot)$ be a L -layer zero-mean Deep GP where $f_L(\cdot)$ has a mean-square continuous stationary prior covariance. Then $\mathbb{E} [DGP(\mathbf{x}) DGP(\mathbf{x}')] > 0$ for all \mathbf{x}, \mathbf{x}' .*

Proof of Theorem 4. Throughout the proof, we will use the shorthand $\mathbf{f}_\ell = f_\ell \circ \dots \circ f_1(\mathbf{x})$ and $\mathbf{f}'_\ell = f_\ell \circ \dots \circ f_1(\mathbf{x}')$. Because $k_L(\cdot, \cdot)$ is stationary, we can express $\mathbb{E} [DGP(\mathbf{x}) DGP(\mathbf{x}')]$ as:

$$\mathbb{E} [DGP(\mathbf{x}) DGP(\mathbf{x}')] = \int k_L(\mathbf{f}_{L-1} - \mathbf{f}'_{L-1}) d\mu(\mathbf{f}_{L-1}, \mathbf{f}'_{L-1}).$$

Moreover, by Bochner's theorem, we can express $k_L(\mathbf{f}_{L-1} - \mathbf{f}'_{L-1})$ as the Fourier transform of some positive finite measure $\mu(\xi)$:

$$\mathbb{E} [DGP(\mathbf{x}) DGP(\mathbf{x}')] = \int \left(\int \exp(i \xi^\top (\mathbf{f}_{L-1} - \mathbf{f}'_{L-1})) d\mu(\xi) \right) d\mu(\mathbf{f}_{L-1}, \mathbf{f}'_{L-1}). \quad (13)$$

Note that $|\exp(i \cdot)|$ is bounded everywhere, and $\mu(\xi)$ and $d\mu(\mathbf{f}_{L-1}, \mathbf{f}'_{L-1})$ are finite measures. Therefore we can switch the orders of integration in Eq. (13):

$$\begin{aligned}\mathbb{E} [DGP(\mathbf{x}) DGP(\mathbf{x}')] &= \int \left(\int \exp(i \xi^\top (\mathbf{f}_{L-1} - \mathbf{f}'_{L-1})) d\mu(\mathbf{f}_{L-1}, \mathbf{f}'_{L-1}) \right) d\mu(\xi). \\ &= \int \left(\int \exp \left(i \begin{bmatrix} \xi \\ -\xi \end{bmatrix}^\top \begin{bmatrix} \mathbf{f}_{L-1} \\ \mathbf{f}'_{L-1} \end{bmatrix} \right) d\mu \left(\begin{bmatrix} \mathbf{f}_{L-1} \\ \mathbf{f}'_{L-1} \end{bmatrix} \right) \right) d\mu(\xi).\end{aligned}\quad (14)$$

Applying the characteristic function lower bound for Deep GP marginals (see Appx. F, Eq. 27):

$$\mathbb{E} [DGP(\mathbf{x}) DGP(\mathbf{x}')] \geq \int \exp \left(-\frac{1}{2} \begin{bmatrix} \xi \\ -\xi \end{bmatrix}^\top \mathbb{E} \left[\begin{bmatrix} \mathbf{f}_{L-1} \\ \mathbf{f}'_{L-1} \end{bmatrix} \begin{bmatrix} \mathbf{f}_{L-1} \\ \mathbf{f}'_{L-1} \end{bmatrix}^\top \right] \begin{bmatrix} \xi \\ -\xi \end{bmatrix} \right) d\mu(\xi). \quad (15)$$

The integrand in Eq. (15) is a real-valued exponential, and so it is strictly positive. Since $\mu(\xi)$ is a positive measure, we have that $\mathbb{E} [DGP(\mathbf{x}) DGP(\mathbf{x}')] > 0$. \square

Theorem 5. Let $k_{\text{lim}}(\mathbf{x}, \mathbf{x}') = \varphi(\|\mathbf{x} - \mathbf{x}'\|_2^2)$ be a mean-square continuous isotropic covariance function that is valid on $\mathbb{R}^D \times \mathbb{R}^D$ for all $D \in \mathbb{N}$. For any width $H_1 \in \mathbb{N}$, the exists a 2-layer Deep GP $f_2(\mathbf{f}_1(\cdot))$ with $\mathbf{f}_1(\cdot) : \mathbb{R}^D \rightarrow \mathbb{R}^{H_1}$ and $f_2(\cdot) : \mathbb{R}^{H_1} \rightarrow \mathbb{R}$ where $\mathbb{E}[f_2(\mathbf{f}_1(\mathbf{x}))f_2(\mathbf{f}_1(\mathbf{x}'))] = k_{\text{lim}}(\mathbf{x}, \mathbf{x}')$.

Proof of Theorem 5. A classic result from Schoenberg [73, Thm. 2] is that, for any mean-square continuous isotropic covariance function $\varphi(\|\mathbf{x} - \mathbf{x}'\|_2^2)$ that is valid on $\mathbb{R}^D \times \mathbb{R}^D$ for all $D \in \mathbb{N}$, there exists some positive finite measure $\mu(\beta)$ such that

$$\varphi(\|\mathbf{x} - \mathbf{x}'\|_2^2) = \int \exp\left(-\frac{1}{2}\|\mathbf{x} - \mathbf{x}'\|_2^2 \beta\right) d\mu(\beta). \quad (16)$$

Let $\text{DGP}^{(1)}(\cdot) = f_2(f_1(\cdot))$ be a 2-layer zero-mean Deep GP with width $H_1 = 1$, and let $k_1(\mathbf{x}, \mathbf{x}') = \mathbf{x}^\top \mathbf{x}'$ and $k_2(z, z') = \int \exp(i \beta(z - z')) d\mu(\beta)$. (By Bochner's theorem, we know that $k_2(\cdot, \cdot)$ is a valid covariance function.) Define $\tau = f_1(\mathbf{x}) - f_1(\mathbf{x}')$. Since $f_1(\mathbf{x})$ and $f_1(\mathbf{x}')$ are jointly Gaussian:

$$p\left(\begin{bmatrix} f_1(\mathbf{x}) \\ f_1(\mathbf{x}') \end{bmatrix}\right) = \mathcal{N}\left(\begin{bmatrix} 0 \\ 0 \end{bmatrix}, \begin{bmatrix} \mathbf{x}^\top \mathbf{x} & \mathbf{x}^\top \mathbf{x}' \\ \mathbf{x}'^\top \mathbf{x} & \mathbf{x}'^\top \mathbf{x}' \end{bmatrix}\right)$$

we have that $p(\tau) = \mathcal{N}(\mathbf{0}, \|\mathbf{x} - \mathbf{x}'\|_2^2)$. Substituting τ into Eq. (14), we have:

$$\begin{aligned} \mathbb{E}\left[\text{DGP}^{(1)}(\mathbf{x}) \text{DGP}^{(1)}(\mathbf{x}')\right] &= \int \left(\int \exp(i \beta \tau) d\mu(\tau) \right) d\mu(\beta). \\ &= \int \exp\left(-\frac{1}{2}\|\mathbf{x} - \mathbf{x}'\|_2^2 \beta\right) d\mu(\beta). \end{aligned} \quad (17)$$

Thus we have a width-1 Deep GP with prior covariance $k_{\text{lim}}(\cdot, \cdot)$. We can extend this construction to 2-layer Deep GP of any width using the additive sequence defined in Eq. (8). \square

D Additional Results

D.1 Comparing Tails of Wider versus Deeper Models

In Sec. 5, we plot $N = 2$ marginal densities of Deep GP to demonstrate how depth and width affect tail properties (Fig. 2). To further demonstrate that Deep GP are heavy tailed and sharply peaked, Fig. 6 displays the *difference* between Deep GP marginal densities and the limiting GP marginal density, i.e.:

$$p_{\text{DGP}}(y_1, y_2 | \mathbf{x}_1, \mathbf{x}_2) - p_{\text{Lim. GP}}(y_1, y_2 | \mathbf{x}_1, \mathbf{x}_2).$$

Red areas correspond to values of \mathbf{y} where the Deep GP has more density, while blue areas correspond to values where the limiting GP has more density. Note that Deep GP of all widths and depths have red values near the $[0, 0]$ mean (corresponding to a sharper peak than the limiting GP) and red values in the upper left and lower right quadrants (corresponding to heavier tails than the limiting GP).

We also note that deeper/narrower models have heavier tails and sharper peaks than shallower/wider models (Fig. 7). The left plot shows the difference between the marginal densities of Depth-3 and Depth-2 Deep GP (with the same first and second moments). The remaining plots show the difference between Depth-2 Deep GP of varying width (again, with the same first and second moments).

D.2 Control Experiment: How Well Does NUTS Sample Deep GP Posteriors?

In order to determine if the NUTS sampler accurately captures Deep GP performance, we perform a control experiment on synthetic data. Specifically, we generate $N = 1000$ datasets from width = 1, width = 2, width = 4, width = 8 Deep GP, sampling these models at randomly-generated \mathbf{x} values in a 4-dimensional input space. Each generating Deep GP has two layers: the first uses a RBF covariance, and the second uses the sum of 1-dimensional RBF covariances. We then train width = 1, width = 2, width = 4, width = 8 Deep GP on each of the generated datasets, using half the data for training and half for testing. Our hypothesis is that width = j models should at least achieve good test set performance on width = j generated datasets.

Fig. 8 displays the test set log likelihood on the generated datasets. We see that width $\in \{2, 4, 8\}$ models tend to achieve similar performance on each of the datasets. On the other hand, the width = 1 models achieve significantly worse test set performance, even on the dataset generated by a width = 1 model. This suggests that the NUTS sampler is unable to converge to good posterior samples for width = 1 models, which may potentially explain the superior performance of width = 2 Deep GP observed in the Sec. 6.1 experiments.

D.3 3-Layer Deep GP and 3-Layer Bayesian Neural Networks

We extend the experiments from Sec. 6.1 to 3-layer Deep GP and Bayesian neural networks. Specifically, we measure the test set log likelihood (Fig. 9 top) and training set kernel fit (Fig. 9 bottom) on 6 regression datasets. The Deep GP models use a standard RBF covariance function for the first layer and sums of 1-dimensional RBF covariances for the second and third layers. The neural networks add an additional $f_3(\cdot) = \frac{1}{\sqrt{H_2}} \mathbf{w}_3^\top \boldsymbol{\sigma}(\cdot) + \beta b_3$ layer on top of the Eq. (1) construction, where H_2 is the width of the second layer and the entries of \mathbf{w}_3, b_3 are i.i.d. unit Gaussian.

We compare models of different width, increasing the width of both hidden layers simultaneously. It is worth noting that changing the width of the first hidden layer affects the prior second moment of the Deep GP/neural network. Therefore, unlike the experiments in Sec. 6.1, we are no longer ensuring that all models are moment-matched. Nevertheless, width has the same effect for 3-layer models as it does for 2-layer models. Width-2 Deep GP almost always outperform all other Deep GP, and neural networks achieve best log likelihood and kernel fit with ≤ 8 hidden units per layer.

D.4 Additional Figures and Tables

We report additional metrics for the experiments in Sec. 6.1. Figs. 10 and 11 report the test set root mean squared error (RMSE) of 2-layer and 3-layer models as a function of width (lower is better). We find that additional width generally harms RMSE. Table 2 reports the test set RMSE for Deep GP of various depth (controlling the first and second prior moments, as in Table 1). Again, depth is generally beneficial with regards to RMSE.

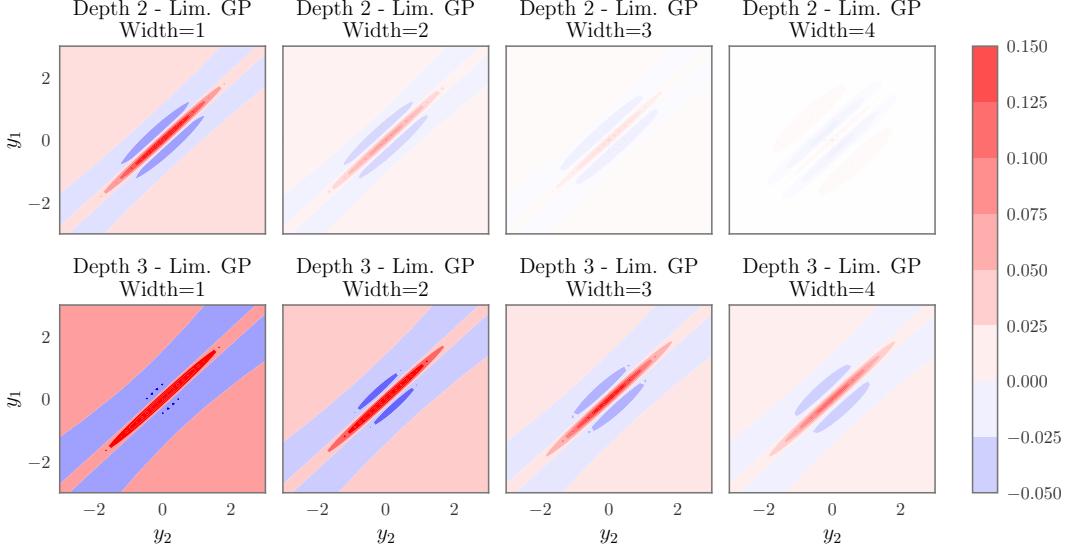


Figure 6: We depict the *difference* between the Deep GP marginal density $p_{\text{DGP}}(y_1, y_2 \mid \mathbf{x}_1, \mathbf{x}_2)$ and the limiting GP marginal density $p_{\text{Lim. GP}}(y_1, y_2 \mid \mathbf{x}_1, \mathbf{x}_2)$ on the $N = 2$ dataset $\mathbf{x}_1 = -0.5$, $\mathbf{x}_2 = 0.5$. Red regions correspond to values of y_1, y_2 where the Deep GP has more density, and vice versa for the blue regions. All Deep GP have heavier tails and a sharper peak than the limiting GP.

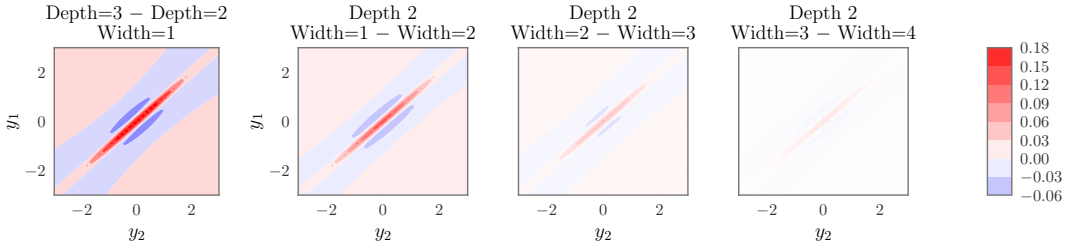


Figure 7: We depict the *difference* between the marginal densities of various Deep GP on the $N = 2$ dataset $\mathbf{x}_1 = -0.5$, $\mathbf{x}_2 = 0.5$. Red regions correspond to values of y_1, y_2 where the deeper/narrower Deep GP has more density, and vice versa for the blue regions. **Left:** Comparing Deep GP of different depth. The 3-layer (width-1) Deep GP has a sharper peak and heavier tails than the 2-layer model, as indicated by the red regions. **Right:** Comparing 2-layer Deep GP of different width. Width- j models have sharper peaks and heavier tails than width- $j + 1$ models, as indicated by the red regions. All models have the same first and second moments.

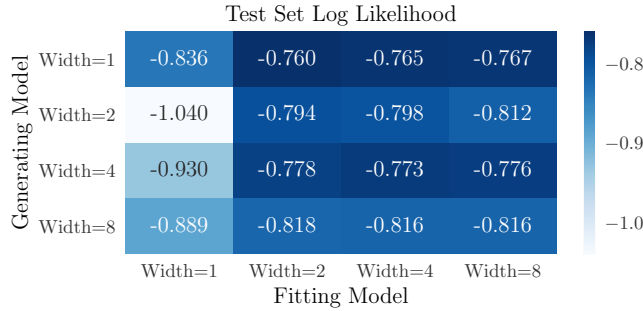


Figure 8: Control experiment to test how well NUTS sampling captures the Deep GP posterior. We generate datasets from width $\in \{1, 2, 4, 8\}$ Deep GP, and then fit width $\in \{1, 2, 4, 8\}$ Deep GP to these datasets. The width $\in \{2, 4, 8\}$ models achieve roughly the same test set log likelihood on each dataset (higher is better). width = 1 Deep GP tend to achieve worse log likelihood, even on a dataset generated from a width = 1 Deep GP.

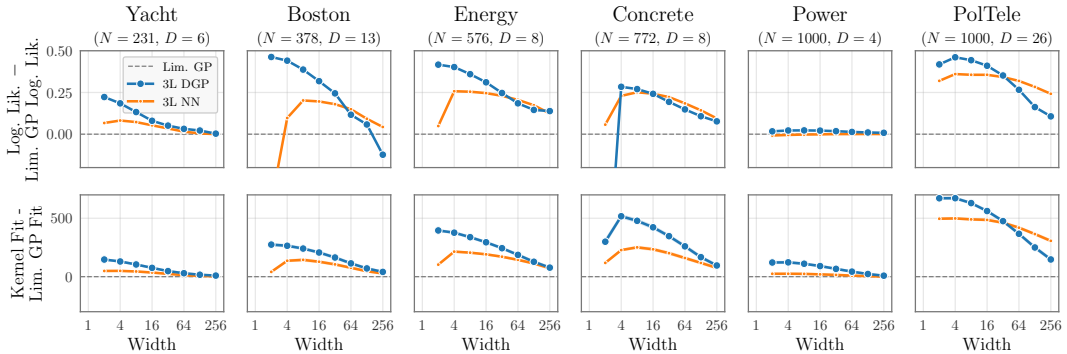


Figure 9: **Top:** Test set log likelihood (LL) of 3-layer Deep GP (and neural networks) as a function of width on regression datasets (higher is better). Numbers are shifted so that 0 corresponds to the limiting GP log likelihood. **Bottom:** Fit of the posterior kernel $k(f_2(f_1(\cdot)), f_2(f_1(\cdot)))$ on the training data, as measured by Gaussian log marginal likelihood (higher is better). 0 corresponds to the limiting GP log marginal likelihood.

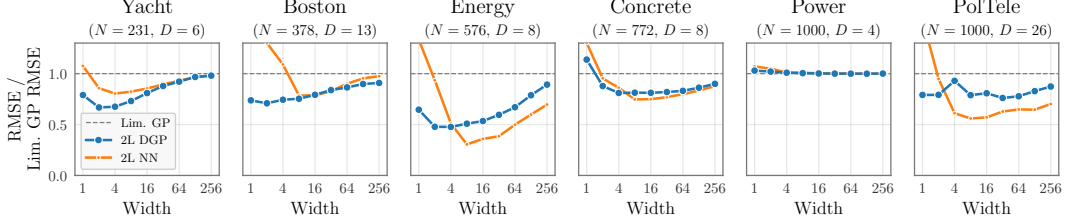


Figure 10: Test set root mean squared error (RMSE) of **2-layer** Deep GP (and neural networks) as a function of width on regression datasets (lower is better). Numbers are scaled so that 1 corresponds to the limiting GP RMSE.

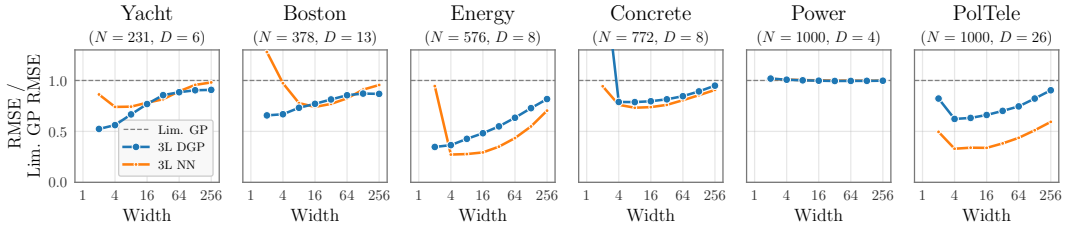


Figure 11: Test set root mean squared error (RMSE) of **3-layer** Deep GP (and neural networks) as a function of width on regression datasets (lower is better). Numbers are scaled so that 1 corresponds to the limiting GP RMSE.

Table 2: Root mean squared error (RMSE) of Deep GP on UCI regression datasets as a function of depth (lower is better). All models for a given dataset have the same prior covariance.

Depth	Yacht ($N = 231, D = 6$)	Boston ($N = 378, D = 13$)	Energy ($N = 576, D = 8$)	Concrete ($N = 772, D = 8$)	Power ($N = 1000, D = 4$)	PolTele ($N = 1000, D = 26$)
1	0.327	0.643	0.267	0.424	0.241	0.305
2	0.240	0.480	0.183	0.350	0.235	0.229
3	0.229	0.426	0.169	0.438	0.236	0.218

E Proof of Theorem 1

Here we prove one of our main results (Thm. 1), which states that Deep GP converge to (single-layer) GP in the infinite width limit. Following Matthews et al. [57], we will prove that random processes with countable index sets converge in distribution to GP with countable index sets. Thus, it is sufficient to prove that the marginals of the random process converge in distribution to multivariate Gaussians [e.g. 13].

Before arriving at a general result, we begin with specialized proofs for two subclasses of Deep GP: 1) those that use *additively-decomposing prior covariance functions* in each GP layer (Observation 1), and 2) those that use *isotropic prior covariance functions* (Observation 2). We note that these two cases include many “textbook” covariance functions (i.e. the kernels described by Genton [36] or Rasmussen and Williams [70, Ch. 4]). Afterwards, we present a more general result. We note that the assumptions required for the general result are rather minimal, and are indeed satisfied by many Deep GP architectures (or arbitrarily-precise approximations thereof).

E.1 Warmup 1: Deep GP with Additive and/or Isotropic Covariance Functions

The first case we will explore is Deep GP with covariance functions that decompose additively. We will assume that the output of the additive composition is scaled to account for the input dimensionality. This additive decomposition suggests a straightforward application of the strong law of large numbers.

Observation 1. Let $f_2(\mathbf{f}_1(\mathbf{x}))$ be a 2-layer zero-mean Deep GP, where $k_2(\cdot, \cdot) : \mathbb{R}^{H_1} \times \mathbb{R}^{H_1} \rightarrow \mathbb{R}$ can be written in the form:

$$k_2(\mathbf{z}, \mathbf{z}') = \frac{1}{H_1} \sum_{i=1}^{H_1} k_2^{(\text{comp})}(z_i, z'_i), \quad (18)$$

where $k_2^{(\text{comp})}(\cdot, \cdot) : \mathbb{R} \times \mathbb{R} \rightarrow \mathbb{R}$ is a positive definite function that is bounded by some polynomial:

$$|k_2^{(\text{comp})}(z, z')| \leq \sum_{i=0}^R \sum_{j=0}^i a_{i,j} |z^{i-j} z'^j|$$

for some $R < \infty$ and constants $a_{i,j} > 0$. Additionally, assume that $|k_1(\mathbf{x}, \mathbf{x}')| < \infty$ for all finite \mathbf{x}, \mathbf{x}' . Then the conditional covariance $\mathbb{E}[f_2(\mathbf{f}_1(\mathbf{x}))f_2(\mathbf{f}_1(\mathbf{x}')) | \mathbf{f}_1(\mathbf{x}), \mathbf{f}_1(\mathbf{x}')]$ becomes almost surely constant as $H_1 \rightarrow \infty$ for finite \mathbf{x}, \mathbf{x}' .

Proof. We have that

$$\begin{aligned} & \lim_{H_1 \rightarrow \infty} \mathbb{E}[f_2(\mathbf{f}_1(\mathbf{x}))f_2(\mathbf{f}_1(\mathbf{x}')) | \mathbf{f}_1(\mathbf{x}), \mathbf{f}_1(\mathbf{x}')] \\ &= \lim_{H_1 \rightarrow \infty} k_2(\mathbf{f}_1(\mathbf{x}), \mathbf{f}_1(\mathbf{x}')) = \lim_{H_1 \rightarrow \infty} \frac{1}{H_1} \sum_{i=1}^{H_1} k_2^{(\text{comp})}(f^{(i)}(\mathbf{x}), f^{(i)}(\mathbf{x}')). \end{aligned} \quad (19)$$

Note that all the $k_2^{(\text{comp})}(f^{(i)}(\mathbf{x}), f^{(i)}(\mathbf{x}'))$ terms are i.i.d. by construction. Moreover, since $k_1(\mathbf{x}, \mathbf{x}')$ is finite for all finite \mathbf{x}, \mathbf{x}' , all moments of $f_1^{(i)}(\mathbf{x}), f_1^{(i)}(\mathbf{x}')$ will also be finite. Using our assumptions on $k_2^{(\text{comp})}(\cdot, \cdot)$, we have:

$$\begin{aligned} \left| \mathbb{E}_{f^{(i)}(\cdot)} \left[k_2^{(\text{comp})}(f^{(i)}(\mathbf{x}), f^{(i)}(\mathbf{x}')) \right] \right| &\leq \mathbb{E}_{f^{(i)}(\cdot)} \left[\left| k_2^{(\text{comp})}(f^{(i)}(\mathbf{x}), f^{(i)}(\mathbf{x}')) \right| \right] \\ &\leq \sum_{j=0}^R \sum_{k=0}^j a_{j,k} \mathbb{E}_{f^{(i)}(\cdot)} \left[\left| f^{(i)}(\mathbf{x})^{j-k} f^{(i)}(\mathbf{x}')^k \right| \right] \\ &\leq \sum_{j=0}^R \sum_{k=0}^j a_{j,k} \sqrt{\mathbb{E}_{f^{(i)}(\cdot)} \left[\left| f^{(i)}(\mathbf{x})^{2j-2k} f^{(i)}(\mathbf{x}')^{2k} \right|^2 \right]} \\ &< \infty. \quad (\text{moments of a } f_1^{(i)}(\mathbf{x}), f_1^{(i)}(\mathbf{x}') \text{ are finite}) \end{aligned}$$

Therefore, we can apply the strong law of large numbers to the limit in Eq. (19) which thus is almost surely constant. \square

Neural networks are one common case of a Deep GP with additive covariance functions. Combining Observation 1 with Lemma 1 gives the classic GP convergence result first discovered by Neal [62]. We note however that, when additive structure exists, we do not need to rely on the covariance perspective of Lemmas 1 and 2, as we can prove GP convergence using the central limit analysis of [49, 57, 62].

E.2 Warmup 2: Deep GP with Isotropic Covariance Functions

The most common Deep GP architectures use RBF or Matérn covariance functions for the GP layers [e.g. 17, 24, 25, 41, 72]. These covariance functions belong to the class of *isotropic kernels*, which are covariances that can be written as a function of Euclidean distance:

$$k(\mathbf{z}, \mathbf{z}') = \varphi(\|\mathbf{z} - \mathbf{z}'\|_2^2).$$

Similar to Observation 1, our analysis of isotropic Deep GP relies on the strong law of large numbers. Again, we will assume that the covariance functions are scaled to account for the input dimensionality.

Observation 2. Define $\mathbb{A} \triangleq \cup_{d=1}^{\infty} (\mathbb{R}^d \times \mathbb{R}^d)$. Let $f_2(\mathbf{f}_1(\mathbf{x}))$ be a 2-layer zero-mean Deep GP, where $k_2(\cdot, \cdot) : \mathbb{A} \rightarrow \mathbb{R}$ is a continuous isotropic kernel that can be written in the form:

$$k_2(\mathbf{z}, \mathbf{z}') = \begin{cases} \varphi((\mathbf{z} - \mathbf{z}')^2) & \mathbf{z}, \mathbf{z}' \in \mathbb{R} \\ \varphi\left(\frac{1}{2}\|\mathbf{z} - \mathbf{z}'\|_2^2\right) & \mathbf{z}, \mathbf{z}' \in \mathbb{R}^2 \\ \varphi\left(\frac{1}{3}\|\mathbf{z} - \mathbf{z}'\|_2^2\right) & \mathbf{z}, \mathbf{z}' \in \mathbb{R}^3 \\ \varphi\left(\frac{1}{4}\|\mathbf{z} - \mathbf{z}'\|_2^2\right) & \mathbf{z}, \mathbf{z}' \in \mathbb{R}^4 \\ \vdots & \end{cases} \quad (20)$$

Additionally, assume that $|k_1(\mathbf{x}, \mathbf{x}')| < \infty$ for all finite \mathbf{x}, \mathbf{x}' . Then the conditional covariance $\mathbb{E}[f_2(\mathbf{f}_1(\mathbf{x}))f_2(\mathbf{f}_1(\mathbf{x}')) | \mathbf{f}_1(\mathbf{x}), \mathbf{f}_1(\mathbf{x}')]$ becomes almost surely constant as $H_1 \rightarrow \infty$ for finite \mathbf{x}, \mathbf{x}' .

Proof. We have that

$$\begin{aligned} & \lim_{H_1 \rightarrow \infty} \mathbb{E}[f_2(\mathbf{f}_1(\mathbf{x}))f_2(\mathbf{f}_1(\mathbf{x}')) | \mathbf{f}_1(\mathbf{x}), \mathbf{f}_1(\mathbf{x}')] \\ &= \lim_{H_1 \rightarrow \infty} k_2(\mathbf{f}_1(\mathbf{x}), \mathbf{f}_1(\mathbf{x}')) = \lim_{H_1 \rightarrow \infty} \varphi\left(\frac{1}{H_1}\|\mathbf{f}_1(\mathbf{x}) - \mathbf{f}_1(\mathbf{x}')\|_2^2\right) \\ &= \varphi\left(\lim_{H_1 \rightarrow \infty} \sum_{i=1}^{H_1} (f_1^{(i)}(\mathbf{x}) - f_1^{(i)}(\mathbf{x}'))^2\right) \end{aligned} \quad (21)$$

where we can move the limit inside $\varphi(\cdot)$ by the continuity assumption. Note that $f_1^{(i)}(\mathbf{x}) - f_1^{(i)}(\mathbf{x}') \stackrel{\text{i.i.d.}}{\sim} \mathcal{N}(0, \sigma^2)$, where $\sigma^2 = k_1(\mathbf{x}, \mathbf{x}) + k_1(\mathbf{x}', \mathbf{x}') - 2k_1(\mathbf{x}, \mathbf{x}')$. Since $k_1(\mathbf{x}, \mathbf{x}')$ is finite—and thus $\sigma^2 = \mathbb{E}[(f_1^{(i)}(\mathbf{x}) - f_1^{(i)}(\mathbf{x}'))^2]$ is finite—Eq. (21) is almost surely constant by the strong law of large numbers. \square

Combining Observation 2 with Lemma 2, we have that Deep GP with isotropic covariance functions become GP in their infinite width limit.

E.3 Assumptions Required for a General Result

We note that the most common Deep GP/neural network architectures either decompose additively or use isotropic covariance functions [1, 2, 17, 25, 72]. In these cases, Observations 1 and 2 are sufficient to prove GP convergence. To prove a more general result, we will need to make an additional set of assumptions about the GP covariance functions. We emphasize that these assumptions are sufficient but not necessary conditions, yet they hold for most Deep GP architectures (or arbitrarily-accurate approximations thereof). Informally, these assumptions are:

- 1) each covariance function “scales reasonably” with the dimensionality of its inputs;
- 2) each covariance function has a *Lesbegue-Stieltjes representation*; and
- 3) each covariance function is *bounded*.

These assumptions are—in practice—very minimal. The first item ensures that the prior covariance doesn’t “blow up” for high-dimensional data (e.g. the covariance does not converge to a constant or a Dirac delta). The second item admits all but the most pathological covariance functions [79]. The last item may at first seem unreasonable, since some common covariance functions are unbounded (e.g. linear kernel, polynomial kernel, etc.). However, we note that many covariance functions are bounded on any compact domain, and therefore from a practical perspective we can approximate any of these unbounded covariances to any arbitrary precision.

Assumption 1 (Covariance functions have Lesbegue-Stieltjes representations with compact spectral support). We assume that all covariance functions $k(\mathbf{z}, \mathbf{z}') : \mathbb{R}^D \times \mathbb{R}^D \rightarrow \mathbb{R}$ can be represented by a Lesbegue-Stieltjes integral of the following form:

$$k(\mathbf{z}, \mathbf{z}') = \int \rho\left(\frac{1}{D} \sum_{i=1}^D \phi(z_i \xi_i - z'_i \xi'_i)\right) d\mu(\boldsymbol{\xi}, \boldsymbol{\xi}'), \quad (22)$$

where

- $\mu(\xi, \xi')$ is a positive definite function of bounded variation and compact support: i.e.: there exists some constant C such that $\mu((\mathbb{R}^D \times \mathbb{R}^D) - ([-C, C]^D \times [-C, C]^D)) = 0$;
- $\phi : \mathbb{R} \rightarrow \mathbb{R}$ is bounded above and below by a polynomial; and
- $\rho(z) : \mathbb{R} \rightarrow \mathbb{R}$ is a continuous function that is finite for all $|z| < \infty$.

We will show that this formulation—though complex—admits additive kernels, isotropic kernels, and most other non-pathological kernels (or arbitrarily-precise approximations thereof).

Assumption 2 (Covariance functions scale with dimensionality). Let $\mathbb{A} = \cup_{d=1}^{\infty} (\mathbb{R}^d \times \mathbb{R}^d)$. We assume that the covariance function $k(\cdot, \cdot) : \mathbb{A} \rightarrow \mathbb{R}$ scales *reasonably with dimensionality*; that is, it can be written in the following form:

$$k(\mathbf{z}, \mathbf{z}') = \begin{cases} k^{(1)}(\mathbf{z}, \mathbf{z}'), & \mathbf{z}, \mathbf{z}' \in \mathbb{R}, \\ k^{(2)}(\mathbf{z}, \mathbf{z}'), & \mathbf{z}, \mathbf{z}' \in \mathbb{R}^2, \\ k^{(3)}(\mathbf{z}, \mathbf{z}'), & \mathbf{z}, \mathbf{z}' \in \mathbb{R}^3, \\ \vdots \end{cases}$$

where the $k^{(j)}(\mathbf{z}, \mathbf{z}')$ satisfy Assumption 1 and are defined recursively:

$$k^{(j)}(\mathbf{z}, \mathbf{z}') = \int \rho \left(\frac{1}{j} \sum_{i=1}^D \phi(z_i \xi_i - z'_i \xi'_i) \right) d\mu_j(\xi, \xi'), \quad \int_{\xi_j, \xi'_j} d\mu_j(\xi, \xi') = d\mu_{j-1}(\xi_{-j}, \xi'_{-j}),$$

In other words, marginalizing out ξ_j, ξ'_j out of the $2j$ -dimensional product measure $d\mu_j(\xi, \xi')$ recovers the $2(j-1)$ -dimensional product measure of $k^{(j-1)}(\cdot, \cdot)$.

E.4 An Exhaustive Discussion About Assumptions 1 and 2

We again reiterate that Assumptions 1 and 2 are not necessary conditions. If more is known about the Deep GP architecture (e.g. all covariance functions are additive or isotropic, etc.), then it is possible to use a smaller and simpler set of assumptions. We nevertheless argue that—in practice, Assumptions 1 and 2 are indeed very general.

All (mean-square continuous) stationary covariance functions can be expressed by Assumption 1. Note that—if we let $d\mu(\cdot, \cdot)$ be atomic—Eq. (22) admits covariance functions of the form:

$$k(\mathbf{z}, \mathbf{z}') = \varphi \left(\frac{1}{D} (\mathbf{z} - \mathbf{z}') \right), \quad (23)$$

where $\varphi(\cdot) : \mathbb{R}^D \rightarrow \mathbb{R}$ is a bounded and continuous positive definite function. This is the form of a mean-square continuous *stationary covariance function* [e.g. 70, Ch. 4].

All but the most pathological non-stationary covariance functions can be expressed (or well-approximated) by Assumption 1. Alternatively, if we instead choose $\rho(\cdot) = \cos(\cdot)$, $\phi(\cdot)$ to be the identity function, and $\mu(\cdot, \cdot)$ to be non-atomic, then Eq. (22) reduces to:

$$k(\mathbf{z}, \mathbf{z}') = \int \cos \left(\frac{1}{D} (\mathbf{z}_i \xi_i - \mathbf{z}'_i \xi'_i) \right) d\mu(\xi, \xi'), \quad (24)$$

This is a Fourier-Stieltjes integral, and almost all (bounded) covariance functions that are encountered in the machine learning literature can be written in this form [36]. Such covariance functions are known as *harmonizable kernels*. Yaglom [79, Sec. 26.4] argues that (bounded) covariance functions that *cannot* be expressed as Fourier-Stieltjes integrals tend to be pathological in nature.

Of course, any covariance function that can be expressed as Eq. (24) is necessarily *bounded*, since $\cos(\cdot)$ is bounded and the measure $\mu(\cdot, \cdot)$ has bounded variation by assumption. The most common unbounded covariance functions are dot-product kernels, such as the linear kernel ($\beta^2 + \mathbf{x}^\top \mathbf{x}'$ for some constant $\beta > 0$) or the “ReLU kernel” ($\beta^2 + \sigma(\mathbf{x})^\top \sigma(\mathbf{x}')$, where $\sigma(\cdot) = \max\{0, \cdot\}$). Importantly, these covariance functions meet the additive structure condition of Observation 1, and so they do not require the general treatment of Assumptions 1 and 2. However, we would also note

that these covariances are bounded on any compact domain, so we can approximate them to arbitrary precision by replacing \mathbf{x} with $\frac{\mathbf{x}}{\|\mathbf{x}\|} \min\{\|\mathbf{x}\|, B\}$ for any $B < \infty$ and similarly for \mathbf{x}' .

The other simplifying assumption is that the spectral measure $\mu(\cdot, \cdot)$ has compact support. Again, even if $k(\cdot, \cdot)$ corresponds to a spectral measure with infinite support, it can often be approximated to an arbitrary precision by replacing ξ with $\frac{\xi}{\|\xi\|} \min\{\|\xi\|, B\}$ for some constant B .

Assumption 2 captures natural ways of scaling to dimensionality. The recursive formula in Assumption 2 is very close to the general form defined in Assumption 1. The $1/j$ term simply prevents the covariance from becoming unbounded or degenerate as $j \rightarrow \infty$. We note that—by choosing the appropriate $\rho(\cdot)$ and $\phi(\cdot)$ function in Eq. (22)—this $1/j$ term can correspond to “natural” scaling rates. For example:

- If $k(\cdot, \cdot)$ is isotropic, then Eq. (22) can take the form:

$$k(\mathbf{z}, \mathbf{z}') = \varphi \left(\frac{1}{D} \sum_{i=1}^D (z_i - z'_i)^2 \right),$$

where $\varphi(\cdot)$ is a continuous positive definite function. We get this form by setting $\rho(\cdot) = \varphi(\cdot)$, $\phi(\cdot) = (\cdot)^2$, and by setting $\mu(\cdot, \cdot)$ to be atomic. This is the scaling of isotropic covariances studied in Appx. E.2.

- If $k(\cdot, \cdot)$ is additive, then Eq. (22) can take the form:

$$k(\mathbf{z}, \mathbf{z}') = \frac{1}{D} \sum_{i=1}^D \int \cos(z_i \xi_i - z'_i \xi'_i) d\mu(\xi_i, \xi'_i).$$

We get this by setting $\rho(\cdot)$ to be the identity and by setting $\phi(\cdot) = \cos(\cdot)$. This is now the sum of 1D harmonizable covariance functions using the scaling studied in Appx. E.1. Again, harmonizable covariances functions include all but the most pathological bounded covariances.

E.5 A General Result

With Assumptions 1 and 2, we show that the conditional covariance of a 2-layer zero-mean Deep GP becomes almost surely constant in the limit of infinite-width.

Lemma 3. *Let $f_2(\mathbf{f}_1(\mathbf{x}))$ be a 2-layer zero-mean Deep GP, where $k_2(\cdot, \cdot)$ satisfies Assumptions 1 and 2. The conditional covariance $\mathbb{E}[f_2(\mathbf{f}_1(\mathbf{x}))f_2(\mathbf{f}_1(\mathbf{x}')) | \mathbf{f}_1(\mathbf{x}), \mathbf{f}_1(\mathbf{x}')]$ becomes almost surely constant as $H_1 \rightarrow \infty$.*

Proof. By Assumptions 1 and 2, the limiting conditional covariance can be written as:

$$\begin{aligned} & \lim_{H_1 \rightarrow \infty} \mathbb{E}[f_2(\mathbf{f}_1(\mathbf{x}))f_2(\mathbf{f}_1(\mathbf{x}')) | \mathbf{f}_1(\mathbf{x}), \mathbf{f}_1(\mathbf{x}')] \\ &= \lim_{H_1 \rightarrow \infty} k_2(\mathbf{f}_1(\mathbf{x}), \mathbf{f}_1(\mathbf{x}')) \\ &= \lim_{H_1 \rightarrow \infty} \int \rho \left(\frac{1}{H_1} \sum_{i=1}^{H_1} \phi \left(f_1^{(i)}(\mathbf{x})\xi_i - f_1^{(i)}(\mathbf{x}')\xi'_i \right) \right) d\mu_{(H_1)}(\xi, \xi'), \quad (\text{Assumptions 1 and 2}) \\ &= \int \rho \left(\lim_{H_1 \rightarrow \infty} \frac{1}{H_1} \sum_{i=1}^{H_1} \phi \left(f_1^{(i)}(\mathbf{x})\xi_i - f_1^{(i)}(\mathbf{x}')\xi'_i \right) \right) d\mu_{(H_1)}(\xi, \xi'), \\ & \quad (\text{dominated convergence, continuity of } \rho(\cdot)) \end{aligned}$$

where dominated convergence holds because $\rho(\cdot)$ is finite for all finite inputs, $\phi(\cdot)$ is bounded above and below by a polynomial, and $\mu_{(H_1)}(\xi, \xi')$ has bounded variation and compact support. Now consider the exponentiated term:

$$\lim_{H_1 \rightarrow \infty} \frac{1}{H_1} \sum_{i=1}^{H_1} \phi \left(f_1^{(i)}(\mathbf{x})\xi_i - f_1^{(i)}(\mathbf{x}')\xi'_i \right). \quad (25)$$

The $f^{(i)}(\cdot)$ terms are i.i.d. zero-mean Gaussian by construction, and have finite variance because $k_1(\cdot, \cdot)$ is finite almost everywhere (Assumption 1). Moreover, the ξ_i and ξ'_i terms are bounded since $d\mu_{(H_1)}(\xi, \xi')$ has compact support (Assumption 1). Consequentially, $f_1^{(i)}(\mathbf{x})\xi_i - f_1^{(i)}(\mathbf{x}')\xi'_i$ are Gaussian random variables with zero mean and bounded variance. Moreover, since $\phi(\cdot)$ is bounded above and below by a polynomial, and the moments of a Gaussian are positive polynomial functions of the covariance, we have that $\text{Var} \left[\phi \left(f_1^{(i)}(\mathbf{x})\xi_i - f_1^{(i)}(\mathbf{x}')\xi'_i \right) \right]$ is bounded, and thus

$$\left| \mathbb{E} \left[\phi \left(f_1^{(i)}(\mathbf{x})\xi_i - f_1^{(i)}(\mathbf{x}')\xi'_i \right) \right] \right| < \infty, \quad \sum_{i=1}^{\infty} \frac{1}{i^2} \text{Var} \left[\phi \left(f_1^{(i)}(\mathbf{x})\xi_i - f_1^{(i)}(\mathbf{x}')\xi'_i \right) \right] < \infty,$$

Applying the strong law of large numbers, we have that Eq. (25), and thus $\mathbb{E}[f_2(\mathbf{f}_1(\mathbf{x}))f_2(\mathbf{f}_1(\mathbf{x}')) \mid \mathbf{f}_1(\mathbf{x}), \mathbf{f}_1(\mathbf{x}')]$, converge to a constant almost surely. \square

The proof of Thm. 1 follows from applying Lemmas 2 and 3.

Theorem 1 (Restated). *Let $f_L \circ \dots \circ \mathbf{f}_1(\mathbf{x})$ be a zero-mean Deep GP (Eq. 2), where each layer satisfies Assumptions 1 and 2. Then $\lim_{H_L \rightarrow \infty} \dots \lim_{H_1 \rightarrow \infty} f_L \circ \dots \circ \mathbf{f}_1(\mathbf{x})$ converges in distribution to a (single-layer) GP.*

Proof. In the two layer case, combining Lemmas 2 and 3 gives us:

$$\lim_{H_1 \rightarrow \infty} \mathbb{E} \left[\exp \left(i \mathbf{t}^\top \mathbf{f}_2 \right) \right] = \exp \left(-\frac{1}{2} \mathbf{t}^\top \mathbb{E} \left[\mathbf{f}_2 \mathbf{f}_2^\top \right] \mathbf{t} \right) \quad \text{for all } \mathbf{t} \in \mathbb{R}^N. \quad (26)$$

Note that this is the characteristic function of a zero-mean multivariate Gaussian with covariance $\mathbb{E} \left[\mathbf{f}_2 \mathbf{f}_2^\top \right]$. Thus by Lévy's continuity theorem, \mathbf{f}_2 converges in distribution to $\mathcal{N}(\mathbf{0}, \mathbb{E} \left[\mathbf{f}_2 \mathbf{f}_2^\top \right])$. Since this is true for any finite marginal \mathbf{f}_2 , the Deep GP $f_2(\mathbf{f}_1(\cdot))$ converges in distribution to a (single-layer) Gaussian process. A simple induction extends this to multiple layers. \square

E.6 Comparison to Agrawal et al. [1].

Agrawal et al. [1, Thm. 8] also study infinite-width limits of Deep GP, though their analysis is restricted to a sub-class of models. Specifically, they focus on infinitely-wide neural networks with finite bottleneck layers—a specific class of Deep GP that they refer to as *bottleneck NNGP*. As the width of the bottleneck layers grow, these models become neural networks with infinite width in all layers. Coupling this with the analysis of infinitely-wide neural networks [49, 57], we have that bottleneck NNGP converge to standard GP in the limit of infinite width. However, the authors note that not every Deep GP can be expressed by the bottleneck NNGP architecture [1, Remark 7], and so their analysis is not sufficient to prove that all Deep GP converge to GP.

It is worth considering whether this strategy can be applied to other architectures—i.e. what Deep GP can be reduced to infinite-width neural networks with bottlenecks. For example, Cutajar et al. [22] study Deep GP with isotropic covariances. They convert each GP layer into neural network-like layers using random Fourier features [69]. However, their model is not exactly equivalent to a neural network, and so the analysis of Agrawal et al. [1] does not immediately apply. Moreover, it is not obvious how to express nonstationary GP as neural network-like architectures with modular width.

Finally, we remark that the strategy of Agrawal et al. [1, Thm. 8] is in some sense the opposite of what is explored in this paper. They and others [22, 29, 31] reduce certain classes of Deep GP to infinitely-wide neural networks with bottlenecks; conversely, we reduce neural networks to Deep GP.

F Proofs of Theorems 2 and 3

Both Thms. 2 and 3 use the same two-step strategy presented for Lemma 1. We will decompose an expectation using the law of total expectation, and then apply Jensen's inequality.

Theorem 2 (Restated). *Let $f_L \circ \dots \circ \mathbf{f}_1(\cdot)$ be a zero-mean Deep GP. Given a finite set of inputs $\mathbf{X} = [\mathbf{x}_1, \dots, \mathbf{x}_N]$, define $\mathbf{f}_\ell = [(f_\ell \circ \dots \circ \mathbf{f}_1(\mathbf{x}_1)), \dots, (f_\ell \circ \dots \circ \mathbf{f}_1(\mathbf{x}_N))]$ for $\ell \in [1, L]$, and define $\mathbf{K}_{\ell|1} = \mathbb{E}_{\mathbf{f}_L} [\mathbf{f}_L \mathbf{f}_L^\top]$. If $\mathbb{E}_{\mathbf{f}_\ell \mid \mathbf{f}_{\ell-1}} [\mathbf{f}_\ell \mathbf{f}_\ell^\top]$ is not constant a.s. for any $\ell \in [2, L]$, then, $p(\mathbf{f}_L = \mathbf{0}) > \mathcal{N}(\mathbf{g} = \mathbf{0}; \mathbf{0}, \mathbf{K}_{\ell|1})$.*

Proof. We first produce a characteristic function bound of \mathbf{f}_L , extending the proof technique in Lemma 1 to multi-layer models:

$$\begin{aligned}
\mathbb{E}_{\mathbf{f}_L} [\exp(i\mathbf{t}^\top \mathbf{f}_L)] &= \mathbb{E}_{\mathbf{F}_1} \left[\mathbb{E}_{\mathbf{F}_2|\mathbf{F}_1} \left[\dots \mathbb{E}_{\mathbf{F}_{L-1}|\mathbf{F}_{L-2}} \left[\mathbb{E}_{\mathbf{F}_L|\mathbf{F}_{L-1}} [\exp(i\mathbf{t}^\top \mathbf{f}_L)] \right] \right] \right] \\
&\quad \text{(law of total expectation)} \\
&= \mathbb{E}_{\mathbf{F}_1} \left[\mathbb{E}_{\mathbf{F}_2|\mathbf{F}_1} \left[\dots \mathbb{E}_{\mathbf{F}_{L-1}|\mathbf{F}_{L-2}} \left[\exp \left(-\frac{1}{2} \mathbf{t}^\top \mathbf{K}_L(\mathbf{F}_{L-1}, \mathbf{F}_{L-1}) \mathbf{t} \right) \right] \right] \right] \\
&\quad \text{(Gaussian characteristic function)} \\
&\geq \exp \left(-\frac{1}{2} \mathbf{t}^\top \mathbb{E}_{\mathbf{F}_1} \left[\mathbb{E}_{\mathbf{F}_2|\mathbf{F}_1} \left[\dots \mathbb{E}_{\mathbf{F}_{L-1}|\mathbf{F}_{L-2}} [\mathbf{K}_L(\mathbf{F}_{L-1}, \mathbf{F}_{L-1})] \right] \right] \mathbf{t} \right) \\
&\quad \text{(Jensen's inequality, strict convexity of exp)} \\
&= \exp \left(-\frac{1}{2} \mathbf{t}^\top \mathbb{E}_{\mathbf{F}_{L-1}} [\mathbf{K}_L(\mathbf{F}_{L-1}, \mathbf{F}_{L-1})] \mathbf{t} \right) = \exp \left(-\frac{1}{2} \mathbf{t}^\top \mathbb{E}_{\mathbf{f}_L} [\mathbf{f}_L \mathbf{f}_L^\top] \mathbf{t} \right) \\
&\quad \text{(law of total expectation)} \\
&= \exp \left(-\frac{1}{2} \mathbf{t}^\top \mathbb{E}_{\mathbf{f}_L} [\mathbf{f}_L \mathbf{f}_L^\top] \mathbf{t} \right) \\
&= \exp \left(-\frac{1}{2} \mathbf{t}^\top \mathbf{K}_{\text{lim}} \mathbf{t} \right) = \mathbb{E}_{\mathbf{g} \sim \mathcal{N}(\mathbf{0}, \mathbf{K}_{\text{lim}})} [\exp(i\mathbf{t}^\top \mathbf{g})]. \tag{27}
\end{aligned}$$

Note that the inequality is strict for some $\mathbf{t} > \mathbf{0}$ because $\mathbb{E}_{\mathbf{f}_\ell|\mathbf{f}_{\ell-1}} [\mathbf{f}_\ell \mathbf{f}_\ell^\top]$ is almost surely not constant by assumption. Thus, we have

$$\begin{aligned}
p(\mathbf{f}_L = \mathbf{0}) &= \int_{\mathbf{f}_L} \mathbb{E} [\exp(i\mathbf{t}^\top \mathbf{f}_L)] d\mathbf{t} \\
&> \int_{\mathbf{g} \sim \mathcal{N}(\mathbf{0}, \mathbf{K}_{\text{lim}})} [\exp(i\mathbf{t}^\top \mathbf{g})] d\mathbf{t} = \mathcal{N}(\mathbf{g} = \mathbf{0}; \mathbf{0}, \mathbf{K}_{\text{lim}}).
\end{aligned}$$

□

It is worth noting that the Jensen gap of the characteristic function cascades with depth. For example, given the 3-layer model $f_3(f_2(f_1(\cdot)))$, we have:

$$\begin{aligned}
\mathbb{E}_{\mathbf{F}_1} \left[\mathbb{E}_{\mathbf{F}_2|\mathbf{F}_1} \left[\exp \left(-\frac{1}{2} \mathbf{t}^\top \mathbf{K}_3 \mathbf{t} \right) \right] \right] &\geq \mathbb{E}_{\mathbf{F}_1} \left[\exp \left(-\frac{1}{2} \mathbf{t}^\top \mathbb{E}_{\mathbf{F}_2|\mathbf{F}_1} [\mathbf{K}_3] \mathbf{t} \right) \right] \\
&\quad \text{CF of 3-layer Deep GP marginal} \quad \text{CF of 2-layer Deep GP marginal} \\
&\geq \exp \left(-\frac{1}{2} \mathbf{t}^\top \mathbb{E}_{\mathbf{F}_1} \left[\mathbb{E}_{\mathbf{F}_2|\mathbf{F}_1} [\mathbf{K}_3] \right] \mathbf{t} \right), \\
&\quad \text{CF of } \mathcal{N}(\mathbf{0}, \mathbb{E}_{\mathbf{F}_1} [\mathbb{E}_{\mathbf{F}_2|\mathbf{F}_1} [\mathbf{K}_3]])
\end{aligned}$$

Consequently, the peaks of deeper models will be sharper than those of shallower models. This is analogous to the tail effects of depth analyzed in Sec. 5.

Theorem 3 (Restated). *Let $\mathbf{t} \in \mathbb{R}^N$. Using the same setup, notation, and assumptions as Thm. 2, the odd moments of $\mathbf{t}^\top \mathbf{f}_L$ are zero and the even moments larger than 2 are super-Gaussian, i.e. $\mathbb{E}_{\mathbf{f}_L} [(\mathbf{t}^\top \mathbf{f}_L)^r] \geq \mathbb{E}_{\mathbf{g} \sim \mathcal{N}(\mathbf{0}, \mathbf{K}_{\text{lim}})} [(\mathbf{t}^\top \mathbf{g})^r]$ for all even $r \geq 4$. Moreover, if $k_L(\cdot, \cdot)$ is bounded almost everywhere, the moment generating function $\mathbb{E}_{\mathbf{f}_L} [\exp(\mathbf{t}^\top \mathbf{f}_L)]$ exists and is similarly super-Gaussian.*

Proof. We can express the moments of $\mathbf{t}^\top \mathbf{f}_L$ as:

$$\mathbb{E}_{\mathbf{f}_L} [(\mathbf{t}^\top \mathbf{f}_L)^r] = \mathbb{E}_{\mathbf{F}_1} \left[\mathbb{E}_{\mathbf{F}_2|\mathbf{F}_1} \left[\dots \mathbb{E}_{\mathbf{F}_{L-1}|\mathbf{F}_{L-2}} \left[\mathbb{E}_{\mathbf{F}_L|\mathbf{F}_{L-1}} [(\mathbf{t}^\top \mathbf{f}_L)^r] \right] \right] \right],$$

and note that the innermost expectation can be simplified to:

$$\mathbb{E}_{\mathbf{f}_L|\mathbf{F}_{L-1}} [(\mathbf{t}^\top \mathbf{f}_L)^r] = \begin{cases} 0 & r \text{ is odd} \\ (\mathbf{t}^\top \mathbf{K}_L(\mathbf{F}_{L-1}, \mathbf{F}_{L-1}) \mathbf{t})^{\frac{r}{2}} (r-1)!! & r \text{ is even.} \end{cases} \tag{Gaussian moments}$$

For odd r , note that this implies $\mathbb{E}_{\mathbf{f}_L}[(\mathbf{t}^\top \mathbf{f}_L)^r] = 0$. For even $r \geq 4$, note that $\mathbf{t}^\top \mathbf{K}_L(\mathbf{F}_{L-1}, \mathbf{F}_{L-1})\mathbf{t} \geq 0$ by positive definiteness of kernels, and note that $(z)^{r/2}$ is convex for all $z \geq 0$. Following the same logic as in the proof for Thm. 2, we have:

$$\begin{aligned} \mathbb{E}_{\mathbf{f}_L}[(\mathbf{t}^\top \mathbf{f}_L)^r] &= \mathbb{E}_{\mathbf{F}_1} \left[\mathbb{E}_{\mathbf{F}_2 | \mathbf{F}_1} \left[\dots \mathbb{E}_{\mathbf{F}_{L-1} | \mathbf{F}_{L-2}} \left[(\mathbf{t}^\top \mathbf{K}_L(\mathbf{F}_{L-1}, \mathbf{F}_{L-1})\mathbf{t})^{\frac{r}{2}} (r-1)!! \right] \right] \right] \\ &\geq \left(\mathbf{t}^\top \mathbb{E}_{\mathbf{F}_1} \left[\mathbb{E}_{\mathbf{F}_2 | \mathbf{F}_1} \left[\dots \mathbb{E}_{\mathbf{F}_{L-1} | \mathbf{F}_{L-2}} [\mathbf{K}_L(\mathbf{F}_{L-1}, \mathbf{F}_{L-1})] \right] \right] \mathbf{t} \right)^{\frac{r}{2}} (r-1)!! \\ &\quad \text{(Jensen's inequality, strict convexity)} \\ &= (\mathbf{t}^\top \mathbf{K}_{\lim} \mathbf{t})^{\frac{r}{2}} (r-1)!! = \mathbb{E}_{\mathcal{N}(\mathbf{g}; \mathbf{0}, \mathbf{K}_{\text{DGP}}(\mathbf{X}, \mathbf{X}))}[(\mathbf{t}^\top \mathbf{g})^r] \end{aligned}$$

A similar proof will show that the moment generating function is similarly super-Gaussian:

$$\begin{aligned} \mathbb{E}_{\mathbf{f}_L}[\exp(\mathbf{t}^\top \mathbf{f}_L)] &= \mathbb{E}_{\mathbf{F}_{L-1}} \left[\exp \left(\frac{1}{2} \mathbf{t}^\top \mathbf{K}_L(\mathbf{F}_{L-1}, \mathbf{F}_{L-1}) \mathbf{t} \right) \right] \quad (28) \\ &= \mathbb{E}_{\mathbf{F}_1} \left[\mathbb{E}_{\mathbf{F}_2 | \mathbf{F}_1} \left[\dots \mathbb{E}_{\mathbf{F}_{L-1} | \mathbf{F}_{L-2}} \left[\exp \left(\frac{1}{2} \mathbf{t}^\top \mathbf{K}_L(\mathbf{F}_{L-1}, \mathbf{F}_{L-1}) \mathbf{t} \right) \right] \right] \right] \\ &\geq \exp \left(\frac{1}{2} \mathbf{t}^\top \mathbb{E}_{\mathbf{F}_1} \left[\mathbb{E}_{\mathbf{F}_2 | \mathbf{F}_1} \left[\dots \mathbb{E}_{\mathbf{F}_{L-1} | \mathbf{F}_{L-2}} [\mathbf{K}_L(\mathbf{F}_{L-1}, \mathbf{F}_{L-1})] \right] \right] \mathbf{t} \right) \\ &= \exp \left(\frac{1}{2} \mathbf{t}^\top \mathbf{K}_{\lim} \mathbf{t} \right) = \mathbb{E}_{\mathcal{N}(\mathbf{g}; \mathbf{0}, \mathbf{K}_{\lim})}[\exp(\mathbf{g}^\top \mathbf{t})]. \end{aligned}$$

We know that the moment generating function exists because, by assumption, $k_L(\cdot, \cdot)$ is bounded almost everywhere, and thus the integral defined by the expectation in Eq. (28) is finite. \square

G Derivation of Deep GP Covariances and Limiting GP Covariances

Here we derive the prior covariances of various Deep GP architectures, as well as the covariances of their corresponding infinite width GP limits.

G.1 RBF + Additive RBF.

First, consider a two layer Deep GP $f_2(\mathbf{f}_1(\cdot))$ where the first layer uses a RBF prior covariance and the second layer uses a sum of 1-dimensional RBF covariances:

$$\begin{aligned} k_1(\mathbf{x}, \mathbf{x}') &= o_1^2 \exp \left(\frac{-\|\mathbf{x} - \mathbf{x}'\|_2^2}{2\ell_1^2} \right), \\ k_2(\mathbf{f}_1(\mathbf{x}), \mathbf{f}_1(\mathbf{x}')) &= \frac{o_2^2}{H_1} \sum_{i=1}^{H_1} \exp \left(-\frac{(f_1^{(i)}(\mathbf{x}) - f_1^{(i)}(\mathbf{x}'))^2}{2\ell_2^2} \right), \end{aligned}$$

where H_1 is the width of the Deep GP, and o_1, ℓ_1, o_2 , and ℓ_2 are hyperparameters. This is the Deep GP architecture most commonly explored in this paper.

To calculate the covariance between $f_2(\mathbf{f}_1(\mathbf{x}))$ and $f_2(\mathbf{f}_1(\mathbf{x}'))$, we first note that $\tau_i \triangleq f_1^{(i)}(\mathbf{x}) - f_1^{(i)}(\mathbf{x}')$ is Gaussian distributed:

$$\tau_i = f_1^{(i)}(\mathbf{x}) - f_1^{(i)}(\mathbf{x}') \sim \mathcal{N}(0, \sigma^2), \quad \sigma^2 \triangleq k_1(\mathbf{x}, \mathbf{x}) + k_1(\mathbf{x}', \mathbf{x}') - 2k_1(\mathbf{x}, \mathbf{x}'). \quad (29)$$

The covariance of the Deep GP is therefore given as:

$$\begin{aligned}
\mathbb{E}_{\text{RBF+add-RBF}}[f_2(\mathbf{f}_1(\mathbf{x}))f_2(\mathbf{f}_1(\mathbf{x}'))] &= \mathbb{E}_{\mathbf{f}_1(\mathbf{x}), \mathbf{f}_1(\mathbf{x}')}[k_2(\mathbf{f}_1(\mathbf{x}), \mathbf{f}_1(\mathbf{x}'))] \\
&= \mathbb{E}_{\tau_i} \left[\frac{o_2^2}{H_1} \sum_{i=1}^{H_1} \exp \left(-\frac{\tau_i^2}{2\ell_2^2} \right), \right] \quad (\tau_i \triangleq f_1^{(i)}(\mathbf{x}) - f_1^{(i)}(\mathbf{x}')) \\
&= \mathbb{E}_{\tau_1} \left[\exp \left(-\frac{\tau_1^2}{2\ell_2^2} \right), \right] \quad (\tau_i \text{ are i.i.d.}) \\
&= \frac{o_2^2}{\sqrt{2\pi\sigma^2}} \int_{-\infty}^{\infty} \exp \left(-\frac{\tau_1^2}{2\ell_2^2} \right) \exp \left(-\frac{\tau_1^2}{2\sigma^2} \right) d\tau_1 \\
&= \frac{o_2^2}{\sqrt{2\pi\sigma^2}} \int_{-\infty}^{\infty} \exp \left(-\tau_1^2 \frac{\sigma^2 + \ell_2^2}{2\sigma^2\ell_2^2} \right) d\tau_1 \\
&= \frac{o_2^2}{\sqrt{2\pi\sigma^2}} \sqrt{\frac{2\pi\sigma^2\ell_2^2}{\sigma^2 + \ell_2^2}}. \quad (\text{Gaussian normalizing constant})
\end{aligned}$$

Plugging in σ^2 from Eq. (29), we have

$$\mathbb{E}_{\text{RBF+add-RBF}}[f_2(\mathbf{f}_1(\mathbf{x}))f_2(\mathbf{f}_1(\mathbf{x}'))] = o_2^2 \left(1 + \frac{2o_1^2 \left(1 - \exp \left(-\frac{\|\mathbf{x} - \mathbf{x}'\|_2^2}{2\ell_1^2} \right) \right)}{\ell_2^2} \right)^{-1/2}. \quad (30)$$

Note that this covariance is the same, regardless of the Deep GP width H_1 . Therefore, it is also the covariance of the infinite width GP limit. More generally, if we replace the first RBF covariance with an arbitrary covariance function $k_1(\cdot, \cdot)$ we have:

$$\mathbb{E}_{k_1+\text{add-RBF}}[f_2(\mathbf{f}_1(\mathbf{x}))f_2(\mathbf{f}_1(\mathbf{x}'))] = o_2^2 \left(1 + \frac{k_1(\mathbf{x}, \mathbf{x}) + k_1(\mathbf{x}', \mathbf{x}') - 2k_1(\mathbf{x}, \mathbf{x}')}{\ell_2^2} \right)^{-1/2}. \quad (31)$$

A similar derivation can be found in [55].

G.2 RBF + (Non-Additive) RBF.

Now consider a two layer Deep GP $f_2(\mathbf{f}_1(\cdot))$ where the first and second layers both use *non-additive* RBF prior covariance functions:

$$\begin{aligned}
k_1(\mathbf{x}, \mathbf{x}') &= o_1^2 \exp \left(-\frac{\|\mathbf{x} - \mathbf{x}'\|_2^2}{2\ell_1^2} \right), \\
k_2(\mathbf{f}_1(\mathbf{x}), \mathbf{f}_1(\mathbf{x}')) &= o_2^2 \exp \left(-\frac{\|\mathbf{f}_1(\mathbf{x}) - \mathbf{f}_1(\mathbf{x}')\|_2^2}{2H_1\ell_2^2} \right),
\end{aligned}$$

where the $1/H_1$ factor is included to reduce the impact of the dimensionality of $\mathbf{f}_1(\cdot)$. This is a very common Deep GP architecture [e.g. 17, 22, 25, 72], and it is the architecture in the Sec. 4 example.

Crucially, the RBF kernel decomposes as a product across its dimensions:

$$k_2(\mathbf{f}_1(\mathbf{x}), \mathbf{f}_1(\mathbf{x}')) = o_2^2 \exp \left(-\frac{\|\mathbf{f}_1(\mathbf{x}) - \mathbf{f}_1(\mathbf{x}')\|_2^2}{2H_1\ell_2^2} \right) = o_2^2 \prod_{i=1}^{H_1} \exp \left(-\frac{\left(f_1^{(i)}(\mathbf{x}) - f_1^{(i)}(\mathbf{x}') \right)^2}{2H_1\ell_2^2} \right)$$

Since the $f_1^{(i)}(\cdot)$ are independent, we have:

$$\begin{aligned}
\mathbb{E}_{\text{RBF+RBF}}[f_2(\mathbf{f}_1(\mathbf{x}))f_2(\mathbf{f}_1(\mathbf{x}'))] &= \mathbb{E}_{\mathbf{f}_1(\mathbf{x}), \mathbf{f}_1(\mathbf{x}')} \left[o_2^2 \prod_{i=1}^{H_1} \exp \left(-\frac{(f_1^{(i)}(\mathbf{x}) - f_1^{(i)}(\mathbf{x}'))^2}{2H_1\ell_2^2} \right) \right] \\
&= o_2^2 \prod_{i=1}^{H_1} \mathbb{E}_{f_1^{(i)}(\mathbf{x}), f_1^{(i)}(\mathbf{x}')} \left[\exp \left(-\frac{(f_1^{(i)}(\mathbf{x}) - f_1^{(i)}(\mathbf{x}'))^2}{2H_1\ell_2^2} \right) \right] \\
&= o_2^2 \prod_{i=1}^{H_1} \mathbb{E}_{\text{RBF+add-RBF}} \left[f_2 \left(\frac{\mathbf{f}_1(\mathbf{x})}{\sqrt{H_1}} \right) f_2 \left(\frac{\mathbf{f}_1(\mathbf{x}')}{\sqrt{H_1}} \right) \right],
\end{aligned}$$

Plugging in Eq. (31), we have

$$\begin{aligned}
\mathbb{E}_{\text{RBF+RBF}}[f_2(\mathbf{f}_1(\mathbf{x}))f_2(\mathbf{f}_1(\mathbf{x}'))] &= o_2^2 \left(1 + \frac{k_1(\mathbf{x}, \mathbf{x}) + k_1(\mathbf{x}', \mathbf{x}') - 2k_1(\mathbf{x}, \mathbf{x}')}{H_1\ell_2^2} \right)^{-H_1/2} \\
&= o_2^2 \left(1 + \frac{2o_1^2 \left(1 - \exp \left(-\frac{\|\mathbf{x} - \mathbf{x}'\|_2^2}{2\ell_1^2} \right) \right)}{H_1\ell_2^2} \right)^{-H_1/2}. \quad (32)
\end{aligned}$$

In the limit as $H_1 \rightarrow \infty$, this second moment becomes:

$$\begin{aligned}
\lim_{H_1 \rightarrow \infty} \mathbb{E}_{\text{RBF+RBF}}[f_2(\mathbf{f}_1(\mathbf{x}))f_2(\mathbf{f}_1(\mathbf{x}'))] &= o_2^2 \exp \left(-\frac{k_1(\mathbf{x}, \mathbf{x}) + k_1(\mathbf{x}', \mathbf{x}') - 2k_1(\mathbf{x}, \mathbf{x}')}{2\ell_2^2} \right) \\
&= o_2^2 \exp \left(\frac{o_1^2}{\ell_2^2} \exp \left(-\frac{\|\mathbf{x} - \mathbf{x}'\|_2^2}{2\ell_1^2} \right) - 1 \right). \quad (33)
\end{aligned}$$

G.3 RBF + Additive RBF + Additive RBF.

Now consider the three layer Deep GP $f_3(\mathbf{f}_2(\mathbf{f}_1(\cdot)))$, where the first layer uses an RBF covariance and the other layers use sums of 1-dimensional RBF covariances.

$$\begin{aligned}
k_1(\mathbf{x}, \mathbf{x}') &= o_1^2 \exp \left(-\frac{\|\mathbf{x} - \mathbf{x}'\|_2^2}{2\ell_1^2} \right), \\
k_2(\mathbf{f}_1(\mathbf{x}), \mathbf{f}_1(\mathbf{x}')) &= \frac{o_2^2}{H_1} \sum_{i=1}^{H_1} \exp \left(-\frac{(f_1^{(i)}(\mathbf{x}) - f_1^{(i)}(\mathbf{x}'))^2}{2\ell_2^2} \right), \\
k_3(\mathbf{f}_2(\mathbf{f}_1(\mathbf{x})), \mathbf{f}_2(\mathbf{f}_1(\mathbf{x}'))) &= \frac{o_3^2}{H_2} \sum_{i=1}^{H_2} \exp \left(-\frac{(f_2^{(i)}(\mathbf{f}_1(\mathbf{x})) - f_2^{(i)}(\mathbf{f}_1(\mathbf{x}')))^2}{2\ell_3^2} \right),
\end{aligned}$$

where H_1, H_2 are the widths of the first and second layers, and $o_1, \ell_1, o_2, \ell_2, o_3$ and ℓ_3 are hyperparameters. We use this architecture in Sec. 5 and Sec. 6.1.

Unfortunately, it is intractable to compute the second moment of this Deep GP in closed form. To see why this is the case, note that:

$$\mathbb{E}_{\text{RBF+add-RBF+add-RBF}}[f_3(\mathbf{f}_2(\mathbf{f}_1(\mathbf{x}))) f_3(\mathbf{f}_2(\mathbf{f}_1(\mathbf{x}')))] = \mathbb{E}_{\mathbf{f}_2(\mathbf{f}_1(\mathbf{x})), \mathbf{f}_2(\mathbf{f}_1(\mathbf{x}'))} [k_3(\mathbf{f}_2(\mathbf{f}_1(\mathbf{x})), \mathbf{f}_2(\mathbf{f}_1(\mathbf{x}')))] \quad (34)$$

In other words, computing the covariance requires taking the expectation over the Deep GP marginal $\mathbf{f}_2(\mathbf{f}_1(\mathbf{x})), \mathbf{f}_2(\mathbf{f}_1(\mathbf{x}'))$ which is intractable to compute. We do note that we can approximate this marginal with Gauss-Hermite quadrature if H_1 is sufficiently small. Moreover, unlike the 2-layer case, the width H_1 affects the second moment of this 3-layer Deep GP. This is because changing H_1 changes the marginal distribution $\mathbf{f}_2(\mathbf{f}_1(\mathbf{x})), \mathbf{f}_2(\mathbf{f}_1(\mathbf{x}'))$, which ultimately impacts the expectation in Eq. (34). Changing the value of H_2 does not affect the covariance by linearity of expectation, assuming that we hold H_1 constant.

As $H_1 \rightarrow \infty$ and $\mathbf{f}_2(\mathbf{f}_1(\cdot))$ converges to a Gaussian process, the expectation in Eq. (34) becomes tractable again. $f_3(\mathbf{f}_2(\mathbf{f}_1(\cdot)))$ effectively becomes a 2-layer Deep GP, where the first layer has covariance given by Eq. (30) and the second layer is the sum of 1-dimensional RBF covariances. Thus, combining Eq. (30) and Eq. (31), we can compute the covariance of the limiting GP:

$$\begin{aligned} & \lim_{H_2 \rightarrow \infty} H_1 \rightarrow \infty \mathbb{E}_{\text{RBF+add-RBF+add-RBF}} [f_3(\mathbf{f}_2(\mathbf{f}_1(\mathbf{x}))) f_3(\mathbf{f}_2(\mathbf{f}_1(\mathbf{x}')))] \\ &= o_3^2 \left(1 + \frac{2o_2 \left(1 - \left(1 + \frac{2o_1^2 \left(1 - \exp \left(-\frac{\|\mathbf{x} - \mathbf{x}'\|_2^2}{2\ell_1^2} \right) \right)}{\ell_2^2} \right)^{-1/2} \right)^{-1/2}}{\ell_3^2} \right) \end{aligned}$$

A similar derivation can be found in [55].

G.4 Neural networks.

The prior second moment of a neural network with ReLU activations and a single hidden layer (i.e. the construction in Eq. 1) is given by the arc-cosine kernel [21]:

$$\mathbb{E}_{\text{2-layer NN}} [f_2(\mathbf{f}_1(\mathbf{x})) f_2(\mathbf{f}_1(\mathbf{x}'))] = \beta^2 + \frac{1}{2\pi} \|\mathbf{x}\| \|\mathbf{x}'\| (\sin(\theta) + (\pi - \theta) \cos(\theta)), \quad (35)$$

where $\theta = \cos^{-1} ((\mathbf{x}^\top \mathbf{x}') / (\|\mathbf{x}\| \|\mathbf{x}'\|))$. Note that this covariance is constant regardless of H_1 .

As with the 3-layer RBF Deep GP, we cannot compute the prior second moment of deeper neural networks in closed form. Moreover, once neural networks have more than 1 hidden layer, then the width of hidden layers affects the covariance. Nevertheless, we can compute the limiting infinite width covariance using the recursive formula defined in [21, 49].

H Experimental Details

The experiments are implemented in PyTorch [66], supplemented by the Pyro [14] and GPyTorch [34] libraries – all of which are open source. We run them on a cluster with GTX1080 and GTX2080 GPU, and we estimate that we use 1000 hours of GPU compute time. The largest experiments (CIFAR10 LeNet and ResNet with maximum width) require 48GB of GPU memory; all other experiments only require $\leq 11\text{GB}$ of memory.

Datasets. The datasets for the regression experiments are from the UCI repository [9]. Unless otherwise stated, we split these datasets into 75% training data, 15% test data, and 10% validation data. For larger datasets, we subsample the training dataset to a maximum of $N = 1000$ data points. All input features are normalized to be between -1 and 1 , and the \mathbf{y} values are z-scored to have 0 mean and unit variance.

For the non-Bayesian neural network experiments, we use the MNIST [48] and CIFAR10 [47] datasets. We z-score the inputs so that each channel has 0 mean and unit variance. We use the standard 10,000 data point test sets, and subsample the remaining data for training.

Deep GP models. All Deep GP models use GP layers with zero prior mean. We perform inference without making any scalable approximations, though we do add a constant diagonal of 10^{-4} to all prior covariances for stability. We perform inference using the NUTS sampler [43] implemented in Pyro [14], using 500 warmup steps, drawing 500 samples, a target acceptance probability of 0.8, an initial learning rate of 0.1, and a maximum tree depth of 10. To improve inference, we infer the “whitened” latent variables $\mathbf{L}_1^{-1}\mathbf{F}_1$ and $\mathbf{L}_2^{-1}\mathbf{f}_2$, where \mathbf{L}_1 and \mathbf{L}_2 are the Cholesky factors of $\mathbf{K}_1(\mathbf{X}, \mathbf{X})$ and $\mathbf{K}_2(\mathbf{F}_1, \mathbf{F}_1)$ respectively. For all width ≥ 2 Deep GP, we initialize the latent variables by running 1000 steps of Adam [46] with learning rate 0.01 on the maximum a posteriori Deep GP objective. Because width-1 Deep GP inference is more challenging (see the control experiment

in Appx. D), we instead initialize the latent variables of these models from the mean of a doubly stochastic variational Deep GP [72], where we use 300 inducing points per layer, 10 function samples, and a minibatch size of 128. We optimize the variational Deep GP with Adam for 2000 iterations, using an initial learning rate of 0.01, dropping it by a factor of 10 after 50% and 75% of training.

For each Deep GP model, we use hyperparameters that maximize the log marginal likelihood of the corresponding limiting GP. To find these hyperparameters, we perform 100 iterations of Adam on the limiting GP using a learning rate of 0.1, initializing all covariance hyperparameters to 1 and initializing the likelihood observational noise to 0.2.

Bayesian neural network models. We train the Bayesian neural networks in a very similar manner. However, we perform 2000 warmup steps and draw 1000 samples using NUTS. Again, we use the same hyperparameters as the optimized limiting GP.

Non-Bayesian neural network models. We construct the models to match Eq. (1)—i.e. we scale the inputs to each layer based on their dimensionality.³ We optimize these models using Adam (SGD for ResNet models) with a learning rate of 0.1, dropping the learning rate by a factor of 10 after 50% and 75% of training. The weight decay parameter is set to correspond to a per-parameter prior of $\mathcal{N}(0, 20)$. We train the models for 20000 iterations (MNIST) and 40000 iterations (CIFAR10) with a minibatch size of 256.

Effect of depth experiments in Sec. 6.1. In these experiments, our goal is to investigate the effects of depth while controlling for the first and second moments of the Deep GP models. To that end, we construct a 3-layer Deep GP, 2-layer Deep GP, and a single-layer GP all with zero mean and the same prior covariance. The 3-layer Deep GP uses a RBF covariance in the first layer, and sums of 1-dimensional RBF kernels in the other two layers. We set the widths to be $H_1 = 2$ and $H_2 = 8$. The 2-layer Deep GP uses a RBF covariance in the first layer with a width of $H_1 = 2$, while the second layer uses the following covariance:

$$o_3^2 \left(1 + \frac{2o_2^2 \left(1 - \frac{1}{H_1} \sum_{i=1}^{H_1} \exp \left(- \left(f_1^{(i)}(\mathbf{x}) - f_1^{(i)}(\mathbf{x}') \right)^2 / (2\ell_2) \right) \right)}{\ell_3^2} \right)^{-1/2}. \quad (36)$$

We empirically confirm that the 2-layer and 3-layer models have the same prior covariance.

For the single layer GP, we compute the covariance of the 3-layer model using the formula in Eq. (34). We approximate the marginal distribution $p(\mathbf{f}_2(\mathbf{f}_1(\mathbf{x})), \mathbf{f}_2(\mathbf{f}_1(\mathbf{x}'))$ using Gauss-Hermite quadrature with 11 nodes. Again, we empirically confirm that the single-layer and 3-layer models have the same prior covariance.

Visualizing $N = 2$ marginal densities in Sec. 5. The 3-layer Deep GP uses a RBF covariance in the first layer, and sums of 1-dimensional RBF kernels in the other two layers. We vary both widths H_1 and H_2 simultaneously, and we set all hyperparameters to 1. The 2-layer Deep GP are designed to match the prior covariance of the width-1 3-layer model. To that end, the first layer uses an RBF covariance, and the second layer uses the following covariance:

$$\frac{1}{H_1} \sum_{i=1}^{H_1} \left(1 + 2 \left(1 - \sum_{i=1}^{H_1} \exp \left(- \frac{\left(f_1^{(i)}(\mathbf{x}) - f_1^{(i)}(\mathbf{x}') \right)^2}{2} \right) \right) \right)^{-1/2}. \quad (37)$$

Again, we empirically verify that these models have the same prior covariance. We approximate the marginal densities at 400 evenly spaced grid points on $\mathbf{y} \in [-3, 3] \times [3, 3]$ using Gauss-Hermite quadrature with 7 nodes.

³We do not perform this scaling on the ResNet models, as this scaling is undone by batch normalization.